

1 Past and future interannual variability of Arctic sea ice in
2 coupled climate models
3

4 John R. Mioduszewski¹, Stephen Vavrus¹, Muyin Wang^{2, 3}, Marika Holland⁴, and Laura Landrum⁴
5
6

7
8 ¹Nelson Institute Center for Climatic Research, University of Wisconsin—Madison, Madison,
9 Wisconsin.

10 ²Joint Institute for the Study of the Atmosphere and Oceans, University of Washington, Seattle,
11 Washington.

12 ³Pacific Marine Environmental Laboratory, National Oceanic and Atmospheric Administration,
13 Seattle, Washington.

14 ⁴National Center for Atmospheric Research, Boulder, Colorado.
15
16
17
18
19
20
21
22
23

24 *Corresponding author: Steve Vavrus, sjvavrus@wisc.edu*
25

26
27
28
29
30
31
32
33
34
35
36
37
38
39
40
41
42
43
44
45
46
47
48
49

Abstract

The diminishing Arctic sea ice pack has been widely studied, but mostly focused on time-mean changes in sea ice rather than on short-term variations that also have important physical and societal consequences. In this study we test the hypothesis that future interannual Arctic sea ice area variability will increase by utilizing 40 independent simulations from the Community Earth System Model's Large Ensemble (CESM-LE) for the 1920-2100 period, and augment this with simulations from 12 models participating in the Coupled Model Intercomparison Project Phase 5 (CMIP5). Both CESM-LE and CMIP5 models project that ice area variability will indeed grow substantially, but not monotonically in every month. There is also a strong seasonal dependence in the magnitude and timing of future variability increases that is robust among CESM ensemble members. The variability in every month is directly correlated with the average ice retreat rate before there is an eventual disappearance in both terms as the ice pack becomes seasonal in summer and autumn by late century. The peak in variability correlates best with the total area of ice between 0.2 - 0.6 m monthly thickness, indicating that substantial future thinning of the ice pack is required before variability maximizes. Within this range, the most favorable thickness for high areal variability depends on the season, especially whether ice growth or ice retreat processes dominate. Thermodynamic melting (top, bottom, lateral) and growth (frazil, congelation) processes are more important than dynamical mechanisms, namely ice export and ridging, in controlling ice area variability.

1. Introduction

Arctic sea ice extent has declined by more than 40% since 1979 during summer (e.g. Stroeve et al. 2012; Serreze and Stroeve 2015; Comiso et al. 2017), primarily as a consequence of greenhouse gas forcing (Notz and Marotzke 2012) but also internal variability (Ding et al. 2017). While this trend is greatest in summer, substantial losses are observed throughout the year (Cavalieri and Parkinson 2012) resulting in an ice season duration that is up to 3 months shorter in some regions (Stammerjohn et al. 2012). Reduced ice area is accompanied by a greater fraction of younger ice (Nghiem et al. 2006; Maslanik et al. 2007a, 2011), which reduces the mean thickness of the basin ice pack (Kwok and Rothrock 2009; Kwok et al. 2009; Lang et al. 2017). As a result, the estimated negative trend in sea ice volume (-27.9% per decade) is about twice as large as the trend in sea ice area (-14.2% per decade; Overland and Wang 2013).

Output from many climate models suggests that the Arctic sea ice cover will not retreat in a steady manner, but will likely fluctuate more as it diminishes, punctuated by occasional Rapid Ice Loss Events (RILEs; Holland et al. 2006; Döscher and Koenigk 2013). The overall decline in ice cover is expected to continue (Collins et al. 2013), and the Arctic may become seasonally ice-free within a few decades, depending on emissions pathway (Stroeve et al. 2007; Wang and Overland 2009; 2012; Massonnet et al. 2012; Wang and Overland 2012; Overland and Wang 2013; Jahn et al. 2016; Notz and Stroeve 2016). However, internal variability confounds prediction of this timing (Stocker et al. 2013; Swart et al. 2015; Jahn et al. 2016; Labe et al. 2018), and even the definition of ice-free differs among Arctic stakeholders (Ridley et al. 2016). Nonetheless, navigation through the Arctic has already increased in frequency as a result of this decline (Melia 2016; Eguíluz et al. 2016), and even more trade routes associated with the increased ice-free season are expected by the end of the 21st century (Aksenov et al. 2015; Stephenson and Smith 2013).

As the Arctic sea ice pack thins and retreats, multi-year ice is being lost and there is consequently a larger proportion of seasonal, thin first-year ice (Kwok et al., 2010, Maykut 1978; Holland et al. 2006). Overall thinner ice may result in an ice pack that exhibits greater inter-annual variability (Maslanik et al. 2007b; Goosse et al. 2009; Notz 2009; Kay et al. 2011; Holland and Stroeve 2011; Döscher and Koenigk 2013), at least partially due to enhanced ice growth and melt (Maykut 1978; Holland et al. 2006; Bathiany et al. 2016a). Decreased ice thickness promotes amplification of a positive ice-albedo feedback, which can magnify sea ice anomalies (Perovich et al. 2007), and thin ice is more vulnerable to anomalous atmospheric forcing and oceanic transport due to the smaller amount of energy required to completely melt the ice (Maslanik et al. 1996, Zhao et al. 2018). For example, pulse-like increases in oceanic heat transport can trigger abrupt ice-loss events in sufficiently thin ice (Woodgate et al. 2012).

Changes in the interannual variability of sea ice have been studied only in a limited capacity, likely because they are only beginning to become visible in September in the present day. Both Goosse et al. (2009) and Swart et al. (2015; their Fig. S6) reported that maximum ice area variability during September occurs once the mean ice extent declines to 3-4 million km². This increased variability may occur due to increased prevalence of RILEs and periods of rapid recovery during this timeframe (Döscher and Koenigk 2013). The thickness distribution during these periods skews toward thinner ice, which is conducive to both rapid ice loss and rapid re-

96 covery processes (Tietsche et al. 2011; Döscher and Koenigk 2013). Holland et al. (2008) con-
97 sidered a critical ice thickness that can serve as a precursor to RILEs, but found it more likely
98 that intrinsic variability played the primary role in the particular RILEs that were studied. More
99 recently, Massonnet et al. (2018) analyzed the projected variability of sea ice *volume* and its pro-
100 jected future change in the CMIP5 ensemble, which suggested a monotonic future decrease. The
101 corresponding variability of sea ice area was investigated by Olonscheck and Notz (2017), but
102 their analysis was much coarser temporally and seasonally, in that it only compared changes be-
103 tween entire blocks of time (the historical 1850-2005 period vs. the future 2006-2100 interval)
104 and was further restricted to the summer and winter seasons.

105
106 Building on these previous studies, our paper has two novel aspects. First, we analyze the
107 transient interannual variability of sea ice area over the course of the year from the early 20th
108 century through the entire 21st century and find very different behavior across the four seasons.
109 These monthly differences are societally important, because marine access to the Arctic will like-
110 ly expand beyond late summer as the ice pack shrinks. Second, we detail how interannual sea ice
111 area variability changes as the ice pack retreats, and we link enhanced future variability to opti-
112 mal ice thicknesses and to the various thermodynamic and dynamic processes that control ice
113 area variability. We analyze a large 40-member ensemble from a single GCM, which allows us
114 to isolate internal variability, which is otherwise muddled with inter-model variability in multi-
115 model comparisons. This allows us to test the hypothesis that inter-annual Arctic sea ice cover
116 variability will increase throughout the year in the future as the ice pack diminishes.

117
118

119 2. Data and Methods

120

121 Ice thickness, concentration, and area were obtained from simulations of the Community
122 Earth System Model Large Ensemble Project (CESM-LE). Ice concentration refers to the per-
123 centage of a given grid cell that is covered by ice, while ice area in this study refers specifically
124 to this percent coverage multiplied by the area of the grid cell yielding a total Arctic ice-covered
125 area. The CESM-LE was designed to enable an assessment of projected change in the climate
126 system while incorporating a wide range of internal climate variability (Kay et al. 2015). It con-
127 sists of 40 ensemble members simulating the period 1920-2100 under historical and projected
128 (RCP8.5 emissions scenario only) external forcing. The ensemble members are produced by in-
129 troducing a small, random round-off level difference in the initial air temperature field for each
130 member. This then generates a consequent ensemble spread that is purely due to simulated inter-
131 nal climate variability. A full description of the CESM-LE is given in Kay et al. (2015), and sim-
132 ilar ensembles using the weaker RCP4.5 and RCP2.6 scenarios can be found in Sanderson et al.
133 (2017, 2018).

134

135 Another data set used in the current study is the model simulations from the Coupled
136 Model Intercomparison Project Phase 5 (CMIP5). Although more than 40 models submitted their
137 simulation results to the Program for Climate Model Diagnosis and Intercomparison (PCMDI),
138 only 12 of them simulated the Arctic sea ice extent both of the monthly means (each individual
139 month) and the magnitude of the seasonal cycle (March minus September sea-ice extent) within
140 20-percent error when compared with observations (Wang and Overland, 2012, Wang and Over-
141 land 2015). Therefore, we used only these 12 models identified by Wang and Overland (2015) in

142 this study: ACCESS1.0, ACCESS1.3, CCSM4, CESM1(CAM5.1), EC-EARTH, HadGEM2-
143 AO, HadGEM2-CC, HadGEM2-ES, MIROC-ESM, MIROC-ESM-CHEM, MPI-ESM-LR, and
144 MPI-ESM-MR. Among the 12 models, half of them use the same sea ice model as CESM-LE
145 (CICE, Hunke and Lipscomb 2010) or a variation of it. If a GCM provided multiple ensemble
146 members, we only kept up to 5 realizations, so that the total ensemble numbers is close to that
147 used in CESM-LE. There are a total of 33 ensemble members from these 12 models in the
148 RCP8.5 emissions scenario. Sea ice area, rather than ice extent, is computed from these 12
149 CMIP5 models to be consistent with CESM-LE results.

150
151 One of our primary analysis datasets is the time series of monthly ice variables. The en-
152 semble mean of all variables is taken after the statistics are calculated for each ensemble mem-
153 ber. 1-year differences in ice area are calculated for each month separately to remove the con-
154 founding effect of amplified variability resulting from a downward trend. Finally, a 10-year run-
155 ning standard deviation is applied to the time series of 1-year differences in monthly ice area,
156 centered on a given year. Ten years was chosen to quantify variability over decadal-scale inter-
157 vals and to provide an adequate number of years for a standard deviation calculation. The timing
158 and magnitude of variability is generally insensitive to the standard deviation window, however,
159 and whether the 1-year difference in ice area or its raw time series is used.

160 161 162 **3. Results**

163 164 **3.1 Sea ice area and its variability**

165
166 Sea ice area in the CESM-LE is projected to decline in all months in the 21st century,
167 proceeding in three phases: a fairly stable regime of extensive coverage in the 20th century, then
168 a decline, followed by virtually no ice remaining in summer and autumn months (Fig. 1). Sea ice
169 area variability follows an analogous three-phase progression in months spanning mid-summer
170 to early winter (Fig. 2). For example, in September this includes a period of modest variability
171 during the 20th century, then a distinct variability peak in the late 2020s and 2030s that coincides
172 with the maximum rate of ice retreat, and finally negligible variability in the late 21st century as
173 the Arctic reaches near ice-free conditions (Fig. 2). The first two phases of this progression in
174 variability occur for months in late winter to early summer (January-June), and suppressed varia-
175 bility would likely emerge beyond the end of the century, assuming that ice cover in these
176 months would continue to retreat. The maximum rate of ice retreat (negative values of the de-
177 rivative) occurs at a different time in the 21st century in each month, occurring presently in Sep-
178 tember but not until the end of the century in spring.

179
180 The same relationship between ice area and its variability is maintained across CMIP5
181 models, though with more noise resulting from the aggregation of many different models rather
182 than ensemble members from a single model (Fig. 3). This is most notable in the sea ice area (1-
183 year difference) time series (Fig. 3, blue), indicating that there is considerable spread in when
184 and how the downward trend proceeds each month, as found in Massonnet et al. (2012), but
185 good agreement that variability increases in this timeframe.

186

187 The analysis of ice area variability in Fig. 2 and Fig. 3 follows that of Goosse et al.
188 (2009) and Swart et al. (2015), but we extend their findings for September to all months and con-
189 firm that the variability in ice area is maximized as its total basin area decline is well underway
190 in both CESM-LE ensembles and across CMIP5 models. A direct relationship between the rate
191 of sea ice retreat and the magnitude of variability is present across all months in CESM-LE and
192 CMIP5: the standard deviation is highest when ice declines the fastest (Figs. 1 and 2). Further-
193 more, the magnitude and timing of peak ice area variability in both sets of experiments differs
194 greatly by season. The peak in magnitude in CESM-LE is most pronounced from November-
195 January when the running standard deviation of ice area exceeds $1 \times 10^6 \text{ km}^2$, while the lowest
196 magnitudes occur in April and May, when the downward trend in ice area does not peak prior to
197 2100 (Fig. 2). Near the end of the 21st century, the running standard deviation also shows an in-
198 crease in the CMIP5 ensembles from December to June (Fig. 3), very similar behavior to that
199 displayed by CESM-LE. However, the magnitude of the increase in the running standard devia-
200 tion in the CMIP5 ensemble mean is smaller than that in CESM-LE. This is not surprising, as the
201 timing of ice retreat varies among models, so averaging them will smooth out the possible sig-
202 nals. The CMIP5 models therefore provide additional evidence that increased variability is asso-
203 ciated with decreasing sea ice coverage.

204
205

206 **3.2 Relationship between ice area variability and thickness**

207

208 Because increasing future concentrations of thin ice are likely a primary factor in in-
209 creased ice area variability, we next consider the relationship between ice thickness and ice area
210 variability in CESM-LE. This is done by correlating the standard deviation of basin-wide ice ar-
211 ea (Fig. 2) with the total area of grid cells with mean ice thickness within a given range for an
212 aggregation of all years and ensemble members, binned at 0.05 m intervals (Fig. 4). 20th century
213 data are omitted because both variables are largely stationary for this period. There is a large dif-
214 ference in the maximum correlation coefficient across seasons, but in most months it peaks be-
215 tween $r = 0.6$ and $r = 0.8$. This peak is associated with the thinnest ice of 0.1 m to 0.2 m from
216 October to January. There is a broad peak in the correlation coefficient between 0.25 m and 0.40
217 m in August and September, while July peaks near 0.45 m thickness but with a weaker maximum
218 correlation coefficient ($r = 0.6$). In June, $r = 0.6$ for most ice thicknesses below 0.8 m, and there
219 is only a weak correlation between these variables in April and May.

220

221 The analysis in Fig. 4 allows us to identify a common range of ice thicknesses when ice
222 area variability generally peaks regardless of the month, which we approximate as 0.2 m to 0.6
223 m. We next track the temporal evolution of this thin ice throughout the basin by calculating the
224 total area of ice that falls within that range. The time-transgressive nature of when the peak in
225 thin ice cover occurs (earliest in September, latest in winter-spring) is consistent with the corre-
226 sponding timing of the peak future sea ice area variability, suggesting that the emergence of a
227 sufficiently thin and contracted ice pack is a primary factor for enhanced ice cover variability
228 (Fig. 5). Both curves match each other in shape, with a steady state early, increasing to a peak
229 and dropping to zero as the Arctic becomes ice-free. The exception is in the spring and early
230 summer when neither increases until the end of the 21st century, when ice begins to decline more
231 rapidly. The two curves are largely in phase as well, with one preceding the other by no more
232 than 10-20 years in July, August, and November–January. The phase difference is due to the

233 chosen range of ice thicknesses, since the best relationship varies by month (Fig. 4). The two
234 curves are in phase from August-October (Fig. 5) when the 0.2 m to 0.6 m range approximates
235 the best relationship between thickness and variability (Fig. 4). However, ice area variability
236 maximizes after the peak in 0.2 m – 0.6 m thickness area in November–January, because varia-
237 bility is more highly correlated with ice slightly thinner than 0.2 m in these months (Fig. 4; Fig.
238 5).

239
240 There are also notable seasonal differences in the spatial pattern of variability during the
241 decade when variability in ice concentration peaks in CESM-LE (Fig. 6). The largest fluctuations
242 occur in a horseshoe-shaped pattern across the Arctic Ocean in autumn, but they are restricted to
243 the boundaries of the Atlantic and Pacific Oceans in late winter and spring. The result is a larger
244 area of high variability in the second half of the year and into January. The mean 0.2 m (dotted)
245 and 0.6 m (solid) ice thickness contours are overlaid for reference (Fig. 6). The contours corre-
246 spond closely to the boundary of maximum variability in ice coverage in most months, which is
247 consistent with results from Fig. 4 and Fig. 5. This demonstrates the first-order relationship be-
248 tween thin ice and the variability of inter-annual ice coverage within a given region.

250 **3.3 Ice concentration tendency**

251
252 The strong relationship between thin ice coverage and high concentration variability oc-
253 curs primarily due to the differing underlying mechanisms controlling ice concentration variabil-
254 ity at a given time, namely whether ice is expanding or retreating. To illustrate this, we chose
255 two months representative of these processes, September and December, to conduct an in-depth
256 analysis of the physical mechanisms involved in the time difference in the two curves in Fig. 5.
257 September is the end of the melt season, and therefore the ice concentration over the entire basin
258 in this month reflects the cumulative impact of melt processes throughout the summer. By con-
259 trast, December is a time of ice growth, particularly in the future, and thus the ice concentration
260 in this month is largely regulated by cumulative growth processes during the autumn. Using
261 available model output, we calculate the ice concentration tendency ($\% \text{ day}^{-1}$) from thermody-
262 namics and dynamics in the regions where the decadal standard deviation of ice concentration
263 exceeds 30% within the grid cell (Fig. S1) to evaluate the mean ice budget. These regions of
264 maximum variability in September and December closely match those in Fig. 6, though the mag-
265 nitude is smaller in Fig. 6 due to the standard deviation being a decadal mean. The daily change
266 in ice concentration is a function of dynamic contributions (ice import/export and ridging), ther-
267 modynamic melt processes (the sum of top, basal, and lateral), and thermodynamic growth (frazil
268 and congelation). Because antecedent conditions of the icepack can be an important factor for
269 determining ice concentration in the month of interest, we sum these terms over the preceding
270 months (July-September or October-December) and report the net 3-month change in ice concen-
271 tration resulting from each component.

272
273 The most interannually variable ice cover during September occurs primarily in the 2020s
274 and is centered across the central Arctic (Fig. S1a), though this region displays net ice expansion
275 in July-September in the 20th century (Fig. 7a) due to rapid ice growth in September. Thermo-
276 dynamic processes dominate over dynamics and are of opposing sign during the 20th century,
277 and thermodynamic processes add an average of 20% to the ice concentration of each grid cell in
278 the region by the end of September, compared with a loss of only 10% from dynamical processes

279 (Fig. 7a). Ice growth diminishes and melt processes accelerate in the early-mid 21st century
280 when the melt processes reduce ice concentration by more than 75% and the dynamic processes
281 essentially disappear with less ice to export (Fig. 7a). After 2060, September ice-free conditions
282 occur, and the thermodynamic term becomes less negative due to reduced areal coverage of ice
283 in June and hence less ice area to melt over the summer (Fig. 7a).
284

285 Because thermodynamic processes dominate in controlling ice concentration in the fu-
286 ture, they should also be the first-order forcing explaining future ice concentration variability,
287 particularly given that the magnitude of the dynamic contribution approaches zero by the 2020s
288 when ice cover is rapidly diminishing. As shown in Figure 7b, the peak interannual variability in
289 the thermodynamic term (red curve) is indeed several times larger than peak variability of the
290 dynamic term (blue curve), and the variability in the thermodynamic term maximizes during the
291 late 2020s in phase with the variability of the ice concentration (green curve) when the thermo-
292 dynamic term is declining most rapidly in Figure 7a. The variability likely also reflects the influ-
293 ence of the surface albedo feedback in amplifying summer ice area variations. There is a second-
294 ary rise in the variability of the thermodynamic term after 2060 (Figure 7b), coinciding with its
295 rapid rise toward zero in Figure 7a, but ice coverage by this point is confined to a diminishing
296 area.
297

298 From the 20th century well into the 21st century, ice growth occurs in the October-
299 December period in a similar region of maximum interannual variability as September, except
300 slightly equatorward (Fig. S1b). Ice export plays a relatively larger role in the regions of interest
301 in December than in September (Fig. 7c). However, the thermodynamic tendency is still the
302 dominant term controlling ice concentration within this region of maximum interannual variabil-
303 ity, and this term increases in the early-mid 21st century to a total of nearly 120%, some of which
304 is offset by ice export that contributes to a 40% decrease in mean ice concentration in the 20th
305 and early 21st centuries (Fig. 7c). The increased net ice growth occurs at this time primarily be-
306 cause there is more initial open water on which frazil ice can form.
307

308 Figure 7d shows that the standard deviation of December ice concentration (green curve) peaks
309 around 2070 and is accompanied by a peak in the variability of the thermodynamic tendency (red
310 curve) of more than double the magnitude of its dynamic tendency (blue curve). A smaller first
311 peak in thermodynamic tendency occurs in the 2020s, when ice growth in this region increases
312 due to increased frazil growth as this region's waters become more open on average in October.
313 This initial peak may be smaller due to the anti-correlation between dynamic and thermodynamic
314 tendency, which reduces the effect of the latter. The rapid subsequent decline in ice growth oc-
315 curs as conditions become too warm for ice growth over much of the October–December period
316 in the 2050s and 2060s (Fig. 7c). This is reflected in the peak in variability of the thermodynamic
317 tendency (red curve) approximately corresponding to the timing of the peak in the ice area varia-
318 bility (green curve) in 2070 (Fig. 7d). The coincidence in their peak variability is similar to that
319 in Figure 7b and underscores the dominance of thermodynamics over dynamics in regulating the
320 variability of ice area.
321

322

323 4. Discussion and Conclusions

324

325 This study has assessed the behavior of interannual Arctic sea ice area variability in the
326 past and future, using a large set of independent realizations from the CESM-LE and simulations
327 from 12 models participating in CMIP5. The results demonstrate the complex, time-varying re-
328 sponse of the ice pack as it transitions from a relatively stable state during the 20th century to a
329 more volatile one. A few of our most important findings are summarized below.

330
331 1) Inter-annual variability of Arctic sea ice cover increases (at least transiently) in all
332 months in the future as sea ice area and thickness decline, but there is a strong seasonal depend-
333 ence. There is also a strong seasonal dependence of the magnitude of the maximum ice area vari-
334 ability in the future, with the greatest magnitude occurring during autumn and winter and small-
335 est during spring by the time the simulation ends in 2100 (Fig. 2-3). The future peak in variabil-
336 ity emerges soonest in late-summer months and latest during spring months, and the magnitude
337 of this peak is positively correlated with the rate of ice loss in every month.

338
339 It is possible that the seasonal differences in ice area variability are partially a construction
340 of the geography of the Arctic Basin, as evident in Fig. 6: when the ice margin is geographically
341 constrained and unable to expand and contract due to a coastline early in the simulation, there is
342 a smaller area subject to high ice variability. This explanation was offered by Goosse et al.
343 (2009) for the same relationship in summer ice area variability, as well as by Eisenman (2010) to
344 explain retreat rate differences between summer and winter. In the future, the ice in the central
345 Arctic Ocean becomes thin enough to expand and contract extensively each season, leading to an
346 increase in variability. Therefore, variability could be considered to be limited particularly in the
347 first phase of its time series (Fig. 2) by the inability of ice to spread across a large open area.
348 Support for this interpretation comes from our calculation of Eisenman's equivalent ice area ap-
349 plied to Fig. 1 (not shown), which resulted in the largest absolute decline in sea ice during the
350 winter-spring months, though summer-autumn ice loss was still greater in relative terms. While
351 useful for approximating potential sea ice extent in the absence of geographic constraints, equiv-
352 alent ice area is still a theoretical construct; our purpose is to assess the variability of ice cover
353 that actually exists. Furthermore, results from Fig. 4 and Fig. 5 suggest that the amount of thin
354 ice alone can explain the evolution of ice variability in every month, though differences in the
355 optimal ice thickness by month may require a partial geographical explanation in addition to one
356 incorporating the components of the thermodynamic tendency of ice area from Fig. 7.

357
358 2) Ice needs to be sufficiently thin before areal variability maximizes, and in CESM-LE the
359 optimal thickness range is generally between 0.2 m to 0.6 m but with some seasonal dependence
360 resulting from the ice melt or ice growth processes that dominate in a given season (Fig. 4-5).
361 The mean ice thickness in late summer and autumn is close to 0.6 m when ice area variability is
362 highest, but is 0.2 m or less for a grid cell average in the winter.

363
364 Increased ice area variability in summer and fall is partly attributable to a higher efficien-
365 cy of open water formation with the thinning sea ice (Holland et al., 2006) and the fact that
366 smaller heating anomalies are required to completely melt through vast areas of the thin ice pack
367 (Bitz and Roe, 2004). We find that the total area of thin ice between the range 0.2 m to 0.6 m is
368 closely related to how soon and how strongly the peak variability in basin-wide ice area emerges,
369 and this is primarily a function of variability in ice area's thermodynamic tendency. This is con-
370 sistent with a physical understanding of this relationship, since ice that is too thin tends to be sea-
371 sonal and melt off every year, whereas thick ice is more likely to survive the melt season. Sea-

372 sonal forecasting of September sea ice coverage takes advantage of this concept, with the fore-
373 cast skill improved when initializing ice thickness up to 8 months in advance (Chevallier et al.,
374 2012; Day et al., 2014).

375
376 In contrast, ice area variability in November-January arises primarily from inter-annual
377 variability in ice growth (as represented by December in Fig. 7c,d), which is dependent on exist-
378 ing open water conditions and temperature anomalies. The peak in ice area variability in these
379 months also coincides with a slightly lower mean ice thickness of 0.2 m, though it is unclear
380 whether that is due to these ice growth rather than melt processes at work during the winter.

381
382 3) Interannual variability in ice concentration is driven primarily by thermodynamic mecha-
383 nisms, which are primarily comprised of either ice growth or ice melt depending on the season.
384 Despite being opposing processes, their magnitudes exceed those of dynamic ice processes (Fig.
385 7).

386
387 The thermodynamic tendency in ice concentration is of much greater magnitude than its
388 dynamic counterpart at both the end of the melt season and start of the growth season, and the
389 maximum interannual variability of the thermodynamic term is mostly in phase with that of ice
390 concentration. The inverse relationship between ice area's interannual variability and its interan-
391 nual rate of change (Figs. 1 and 2) is also found between the thermodynamic tendency and its
392 rate of change (not shown, but inferred from Fig. 7). This is further evidence that ice area varia-
393 bility is primarily driven by thermodynamic processes in the icepack.

394
395 The dominance of the thermodynamic tendency is unsurprising and has been established as
396 the relatively more important set of processes controlling sea ice variability, primarily via
397 transport of mid-latitude eddy heat flux anomalies (Kelleher and Screen, 2018), anticyclone pas-
398 sage (Wernli and Lukas, 2018), and increased ocean heat transport (Li et al., 2018). However,
399 the dynamic contribution to changes in ice concentration can likely be substantial in the absence
400 of regional and monthly averaging, and numerous mechanisms have been described that can
401 generate increased ice transport. Recent examples include divergent ice drift events connected to
402 anomalous circulation patterns (Zhao et al., 2018) as well as the collapse of the Beaufort High
403 (Petty, 2018; Moore et al., 2018), both of which may become more common in the future due to
404 preconditioning of the icepack and further intrusion of mid-latitude cyclones into the Arctic.

405
406 This study offers a unique contribution by focusing on the projected transient evolution
407 of Arctic sea ice variability throughout the year, as characterized by its response to external
408 greenhouse forcing superimposed on short-term internal variability. A recent study (Olonscheck
409 and Notz, 2017) also identified an overall increase in projected variability of summertime sea ice
410 area in CMIP5, but this conclusion was not consistent across all models, possibly because the
411 analysis did not incorporate the pronounced changes in variability over time as the ice pack di-
412 minishes. Increased inter-annual variability in the CESM Large Ensemble as sea ice declines
413 most rapidly is an important result that needs to be accounted for as the ice-free season expands
414 and the timing of maximum variability shifts from September. We also confirm that this relation-
415 ship is maintained across CMIP5 models, suggesting that the responsible mechanisms reported
416 here may apply more generally. These results have important implications for marine navigation
417 going forward, indicating that the otherwise auspicious transition to diminished sea ice in every

418 month may be accompanied by a confounding increase in inter-annual variability of the ice cover
419 before the ice disappears completely.

420

421

422

423 **Acknowledgements**

424

425 We thank two anonymous reviewers for their helpful comments. Support was provided by the
426 NOAA Climate Program Office under Climate Variability and Predictability Program grant
427 NA15OAR4310166. This project is partially funded by the Joint Institute for the Study of the
428 Atmosphere and Ocean (JISAO) under NOAA Cooperative Agreement NA10OAR4320148,
429 contribution number 2017-087, the Pacific Marine Environmental Laboratory contribution num-
430 ber 4671. We would like to acknowledge high-performance computing support from Yellow-
431 stone (ark:/85065/d7wd3xhc) provided by NCAR's Computational and Information Systems La-
432 boratory, sponsored by the National Science Foundation.

433

434

435 **References**

- 436
- 437 Aksenov, Y., E. E. Popova, A. Yool, A. J. G. Nurser, T. D. Williams, L. Bertino, and J. Bergh:
438 On the future navigability of Arctic sea routes: High-resolution projections of the Arctic
439 Ocean and sea ice, *Mar. Policy*, 1–18, doi:10.1016/j.marpol.2015.12.027, 2015.
- 440 Bathiany, S., B. van der Bolt, M. S. Williamson, T. M. Lenton, M. Scheffer, E. H. van Nes, and
441 D. Notz: Statistical indicators of Arctic sea-ice stability – prospects and limitations,
442 *Cryosph.*, 10(4), 1631–1645, doi:10.5194/tc-10-1631-2016, 2016.
- 443 Bitz, C. M., and G. H. Roe: A mechanism for the high rate of sea ice thinning in the Arctic
444 Ocean, *J. Clim.*, 17(18), 3623–3632, doi:10.1175/1520-0442(2004)017, 2004.
- 445 Cavalieri, D. J., and C. L. Parkinson: Arctic sea ice variability and trends, 1979–2010, *Cryosph.*,
446 6(4), 881–889, doi:10.5194/tc-6-881-2012, 2012.
- 447 Collins, M. et al.: Long-term Climate Change: Projections, Commitments and Irreversibility.
448 Intergovernmental Panel on Climate Change, 108, 2013.
- 449 Comiso, J. C., W. N. Meier, and R. Gersten: Variability and trends in the Arctic Sea ice cover:
450 Results from different techniques, *J. Geophys. Res. Ocean.*, 122, 1–22,
451 doi:10.1002/2017JC012768, 2017.
- 452 Ding, Q., et al., Influence of high-latitude atmospheric circulation changes on summertime
453 Arctic sea ice, *Nat. Clim. Chang.*, 7, 289-295, doi:10.1038/nclimate3241, 2017.
- 454 Döscher, R., and T. Koenigk: Arctic rapid sea ice loss events in regional coupled climate
455 scenario experiments, *Ocean Sci. Discuss.*, 9(4), 2327–2373, doi:10.5194/osd-9-2327-
456 2012, 2012.
- 457 Goose, H., O. Arzel., C.M. Bitz, A. de Montety, and M. Vancoppenolle: Increased variability of
458 the Arctic summer ice extent in a warmer climate, *Geophys. Res. Lett.*, 36, L23702,
459 doi :10.1029/2009GL040546, 2009.
- 460 Holland, M. M., C. M. Bitz, and B. Tremblay: Future abrupt reductions in the summer Arctic sea
461 ice, *Geophys. Res. Lett.*, 33(23), 1–5, doi:10.1029/2006GL028024, 2006.
- 462 Holland, M. M., C. M. Bitz, L. B. Tremblay, and D. A. Bailey: The role of natural versus forced
463 change in future rapid summer Arctic ice loss. Arctic sea ice decline: Observations,
464 projections, mechanisms, and implications, E.T. DeWeaver, C.M. Bitz, and L.B.
465 Tremblay, Eds., *Geophysical Monograph Series*, American Geophysical Union,
466 Washington, 133-150 doi:10.1029/180GM10, 2008.
- 467 Holland, M. M., and J. Stroeve: Changing seasonal sea ice predictor relationships in a changing
468 Arctic climate, *Geophys. Res. Lett.*, 38, L18501, doi:10.1029/2011GL049303, 2011.
- 469 Jahn, A., J. E. Kay, M. M. Holland, and D. M. Hall: How predictable is the timing of a summer
470 ice-free Arctic?, *Geophys. Res. Lett.*, 1–8, doi:10.1002/2016GL070067, 2016.
- 471 Eguíluz, V. M., J. Fernández-Gracia, X. Irigoien, and C. M. Duarte: A quantitative assessment of
472 Arctic shipping in 2010–2014, *Sci. Rep.*, 6(August), 30682, doi:10.1038/srep30682,
473 2016.
- 474 Eisenman, I.: Geographic muting of changes in the Arctic sea ice cover, *Geophys. Res. Lett.*,
475 37(16), doi:10.1029/2010GL043741, 2010.
- 476 Hunke, E. C., and W. H. Lipscomb: CICE: The Los Alamos sea ice model, documentation and
477 software user’s manual, version 4.1. Los Alamos National Laboratory Tech. Rep. LACC-
478 06-012, 76 pp., 2010.
- 479 Kay, J. E. et al.: The Community Earth System Model (CESM) Large Ensemble Project: A
480 Community Resource for Studying Climate Change in the Presence of Internal Climate

481 Variability, *Bull. Am. Meteorol. Soc.*, 96(8), 1333–1349, doi:10.1175/BAMS-D-13-
482 00255.1, 2015.

483 Kay, J. E., M. M. Holland, and A. Jahn: Inter-annual to multi-decadal Arctic sea ice extent trends
484 in a warming world. *Geophys. Res. Lett.*, 38, L15708, doi:10.1029/2011GL048008,
485 2011.

486 Kelleher, M., and J. Screen: Atmospheric precursors of and response to anomalous Arctic sea ice
487 in CMIP5 models, *Adv. Atmos. Sci.*, 35(27), doi.org/10.1007/s00376-017-7039-9.

488 Khon, V. C., I. I. Mokhov, M. Latif, V. A. Semenov, and W. Park: Perspectives of Northern Sea
489 Route and Northwest Passage in the twenty-first century, *Clim. Change*, 100(3), 757–
490 768, doi:10.1007/s10584-009-9683-2, 2010.

491 Kwok, R., and D. A. Rothrock: Decline in Arctic sea ice thickness from submarine and ICESat
492 records: 1958–2008, *Geophys. Res. Lett.*, 36(15), doi:10.1029/2009GL039035.

493 Kwok, R., G. F. Cunningham, M. Wensnahan, I. Rigor, H. J. Zwally, and D. Yi: Thinning and
494 volume loss of the Arctic Ocean sea ice cover: 2003–2008, *J. Geophys. Res. Ocean.*,
495 114(7), 2003–2008, doi:10.1029/2009JC005312, 2009.

496 Kwok, R., L.T. Pedersen, P. Gudmandsen, and S. S. Pang: Large sea ice outflow into the Nares
497 strait in 2007, *geophys. Res. Lett.*, 37, L03502, DOI:10.1029/2009GL041872, 2010.

498 Labe, Z., Magnusdottir, G., and H. Stern: Variability of Arctic Sea Ice Thickness Using
499 PIOMAS and the CESM Large Ensemble, *J. Climate*, 31, 3233–3247,
500 [DOI.ORG/10.1175/JCLI-D-17-0436.1](https://doi.org/10.1175/JCLI-D-17-0436.1), 2018.

501 Lang, A., S. Yang, and E. Kaas: Sea ice thickness and recent Arctic warming, *Geophys. Res.*
502 *Lett.*, 44, doi:10.1002/2016GL071274, 2017.

503 Li, D., R. Zhang, and T. Knutson: Comparison of Mechanisms for Low-Frequency Variability of
504 Summer Arctic Sea Ice in Three Coupled Models, *J. Climate*, 31, 1205–
505 1226, [DOI.ORG/10.1175/JCLI-D-16-0617.1](https://doi.org/10.1175/JCLI-D-16-0617.1), 2018.

506 Maslanik, J. A., M. C. Serreze, and R. G. Barry: Recent decreases in Arctic summer ice cover
507 and linkages to atmospheric circulation anomalies, *Geophys. Res. Lett.*, 23(13), 1677–
508 1680, doi:10.1029/96GL01426, 1996.

509 Maslanik, J., S. Drobot, C. Fowler, W. Emery, and R. Barry: On the Arctic climate paradox and
510 the continuing role of atmospheric circulation in affecting sea ice conditions, *Geophys.*
511 *Res. Lett.*, 34(3), 2–5, doi:10.1029/2006GL028269, 2007a.

512 Maslanik, J. A., C. Fowler, J. Stroeve, S. Drobot, J. Zwally, D. Yi, and W. Emery: A younger,
513 thinner Arctic ice cover: Increased potential for rapid, extensive sea-ice loss, *Geophys.*
514 *Res. Lett.*, 34(24), 2004–2008, doi:10.1029/2007GL032043, 2007b.

515 Maslanik, J., J. Stroeve, C. Fowler, and W. Emery: Distribution and trends in Arctic sea ice age
516 through spring 2011, *Geophys. Res. Lett.*, 38(13), 2–7, doi:10.1029/2011GL047735,
517 2011.

518 Massonnet, F., T. Fichefet, H. Goosse, C. M. Bitz, G. Philippon-Berthier, M. M. Holland, and P.
519 Y. Barriat: Constraining projections of summer Arctic sea ice, *Cryosphere*, 6(6), 1383–
520 1394, doi:10.5194/tc-6-1383-2012, 2012.

521 Massonnet, F., M. Vancoppenolle, H. Goosse, D. Docquier, T. Fichefet, and E. Blanchard-
522 Wrigglesworth: Arctic sea-ice change tied to its mean state through thermodynamic
523 processes. *Nat. Clim. Change*, 8, 599–603, 2018.

524 Maykut, G. A.: Energy exchange over young sea ice in the central Arctic, *J. Geophys. Res.*,
525 83(C7), 3646, doi:10.1029/JC083iC07p03646, 1978.

526 Melia, N., K. Haines, and E. Hawkins: Sea ice decline and 21st century trans-Arctic shipping
527 routes, *Geophys. Res. Lett.*, 43(18), 9720–9728, doi:10.1002/2016GL069315, 2016.

528 Moore, G. W. K., Schweiger, A., Zhang, J., and M. Steele: Collapse of the 2017 winter Beaufort
529 High: A response to thinning sea ice? *Geophysical Research Letters*, 45, 2860–2869,
530 doi.org/10.1002/2017GL076446, 2018

531 Nghiem, S. V., I. G. Rigor, D. K. Perovich, P. Clemente-Colón, J. W. Weatherly, and G. Neu-
532 mann: Rapid reduction of Arctic perennial sea ice, *Geophys. Res. Lett.*, 34(19), 1–6,
533 doi:10.1029/2007GL031138, 2007.

534 Notz, D.: The future of ice sheets and sea ice: between reversible retreat and unstoppable loss.,
535 *Proc. Natl. Acad. Sci. U. S. A.*, 106(49), 20590–5, doi:10.1073/pnas.0902356106, 2009.

536 Notz, D., and J. Marotzke: Observations reveal external driver for Arctic sea-ice retreat,
537 *Geophys. Res. Lett.*, 39(8), 1–6, doi:10.1029/2012GL051094, 2012.

538 Notz, D., and J. Stroeve: Observed Arctic sea-ice loss directly follows anthropogenic CO₂
539 emission, *Science*, 354(6313), 747–750, doi:10.1126/science.aag2345, 2016.

540 Olonscheck, D., and D. Notz: Consistently estimating internal variability from climate model
541 simulations. *J. Clim.*, 30, 9555–9573, 2017.

542 Overland, J. E., and M. Wang: When will the summer Arctic be nearly sea ice free?, *Geophys.*
543 *Res. Lett.*, 40(10), 2097–2101, doi:10.1002/grl.50316, 2013.

544 Perovich, D. K., B. Light, H. Eicken, K. F. Jones, K. Runciman, and S. V. Nghiem: Increasing
545 solar heating of the Arctic Ocean and adjacent seas, 1979–2005: Attribution and role in
546 the ice-albedo feedback, *Geophys. Res. Lett.*, 34(19), 1–5, doi:10.1029/2007GL031480,
547 2007.

548 Petty, A. A.: A possible link between winter Arctic sea ice decline and a collapse of the Beaufort
549 High? *Geophysical Research Letters*, 45, 2879–2882,
550 [DOI.ORG/10.1002/2018GL077704](https://doi.org/10.1002/2018GL077704), 2018.

551 Ridley, J. K., R. A. Wood, A. B. Keen, E. Blockley, and J. A. Lowe: Brief Communication:
552 Does it matter exactly when the Arctic will become ice-free?, *Cryosph. Discuss.*,
553 (March), 1–4, doi:10.5194/tc-2016-28, 2016.

554 Sanderson, B. M., Xu, Y., Tebaldi, C., Wehner, M., O'Neill, B., Jahn, A., Pendergrass, A. G.,
555 Lehner, F., Strand, W. G., Lin, L., Knutti, R., and Lamarque, J. F.: Community climate
556 simulations to assess avoided impacts in 1.5 and 2 °C futures, *Earth Syst. Dynam.*, 8,
557 827–847, <https://doi.org/10.5194/esd-8-827-2017>, 2017.

558 Sanderson, B. M., K. W. Oleson, W. G. Strand, F. Lehner, and B. C. O'Neill: A new ensemble of
559 GCM simulations to assess avoided impacts in a climate mitigation scenario. *Clim.*
560 *Change*, 146(3–4), 303–318, 2018.

561 Serreze, M. C., and J. C. Stroeve: Arctic sea ice trends, variability and implications for seasonal
562 ice forecasting, *Philos. Trans. R. Soc. A Math. Phys. Eng. Sci.*, 373(2045), 20140159,
563 doi:10.1098/rsta.2014.0159, 2015.

564 Stephenson, S. R., L. C. Smith, L. W. Brigham, and J. A. Agnew: Projected 21st-century
565 changes to Arctic marine access, *Clim. Change*, 118(3–4), 885–899, doi:10.1007/s10584-
566 012-0685-0, 2013.

567 Stammerjohn, S., R. Massom, D. Rind, and D. Martinson: Regions of rapid sea ice change: An
568 inter-hemispheric seasonal comparison, *Geophys. Res. Lett.*, 39(6), L06501,
569 doi:10.1029/2012GL050874, 2012.

570 Stroeve, J. C., M. C. Serreze, M. M. Holland, J. E. Kay, J. Malanik, and A. P. Barrett: The
571 Arctic's rapidly shrinking sea ice cover: a research synthesis, *Clim. Change*, 110(3–4),
572 1005–1027, doi:10.1007/s10584-011-0101-1, 2012.

573 Stroeve, J., M. M. Holland, W. Meier, T. Scambos, and M. Serreze: Arctic sea ice decline: Faster
574 than forecast, *Geophys. Res. Lett.*, 34(9), 1–5, doi:10.1029/2007GL029703, 2007.

575 Swart, N. C., J. C. Fyfe, E. Hawkins, J. E. Kay, and A. Jahn: Influence of internal variability on
576 Arctic sea-ice trends, *Nat. Clim. Chang.*, 5(2), 86–89, doi:10.1038/nclimate2483, 2015.

577 Tietsche, S., D. Notz, J. H. JungCLAUS, and J. Marotzke: Recovery mechanisms of Arctic summer
578 sea ice, *Geophys. Res. Lett.*, 38(2), 1–4, doi:10.1029/2010GL045698, 2011.

579 Wang, M., and J. E. Overland: A sea ice free summer Arctic within 30 years? *Geophys. Res.*
580 *Lett.*, 36, L07502, doi:10.1029/2009GL037820, 2009.

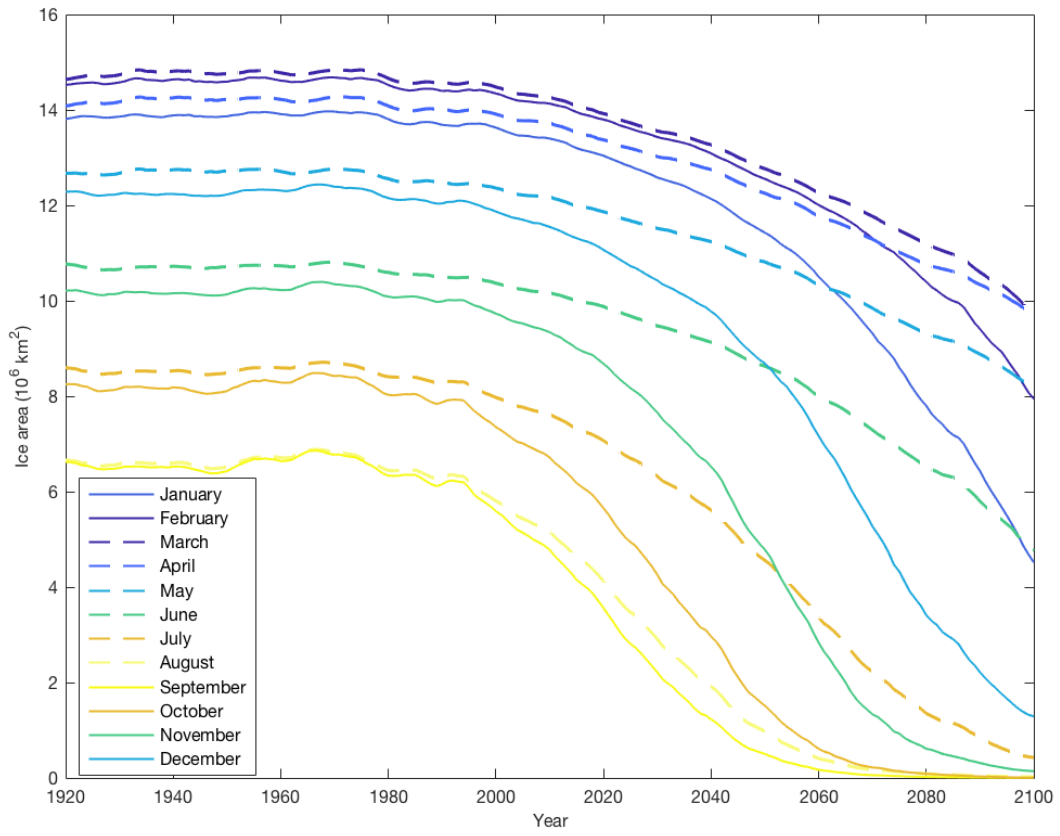
581 Wang, M., and J. E. Overland: A sea ice free summer Arctic within 30 years: An update from
582 CMIP5 models, *Geophys. Res. Lett.*, 39(18), doi:10.1029/2012GL052868, 2012.

583 Wang, M., and J. E. Overland: Projected future duration of the sea-ice-free season in the Alaskan
584 Arctic, *Prog. Oceanogr.*, 136, 50–59, doi:10.1016/j.pocean.2015.01.001, 2015.

585 Wernli, H., and L. Papritz: Role of polar anticyclones and mid-latitude cyclones for Arctic
586 summertime sea-ice melting, *Nat. Geos.*, 11, 108–113, doi:10.1038/s41561-017-0041-0,
587 2018.

588 Woodgate, R. A., T. J. Weingartner, and R. Lindsay: Observed increases in Bering Strait oceanic
589 fluxes from the Pacific to the Arctic from 2001 to 2011 and their impacts on the Arctic
590 Ocean water column, *Geophys. Res. Lett.*, 39, L24603, doi:10.1029/2012GL054092,
591 2012.

592 Zhao, J., D. Barber, S. Zhang, Q. Yang, X. Wang, and H. Xie: Record Low Sea-Ice
593 Concentration in the Central Arctic during Summer 2010, *Adv. Atmos. Sci.*, 35(January),
594 106–115, doi:10.1007/s00376-017-7066-6, 2018.



595 **Figure 1:** The CESM-LE ensemble mean time series of monthly sea ice area (km² x 10⁶).
 596
 597
 598

599
600
601
602
603
604
605
606
607
608
609
610
611
612
613
614
615
616
617
618
619
620
621
622
623
624
625
626
627
628
629
630
631
632
633
634
635
636
637
638
639
640

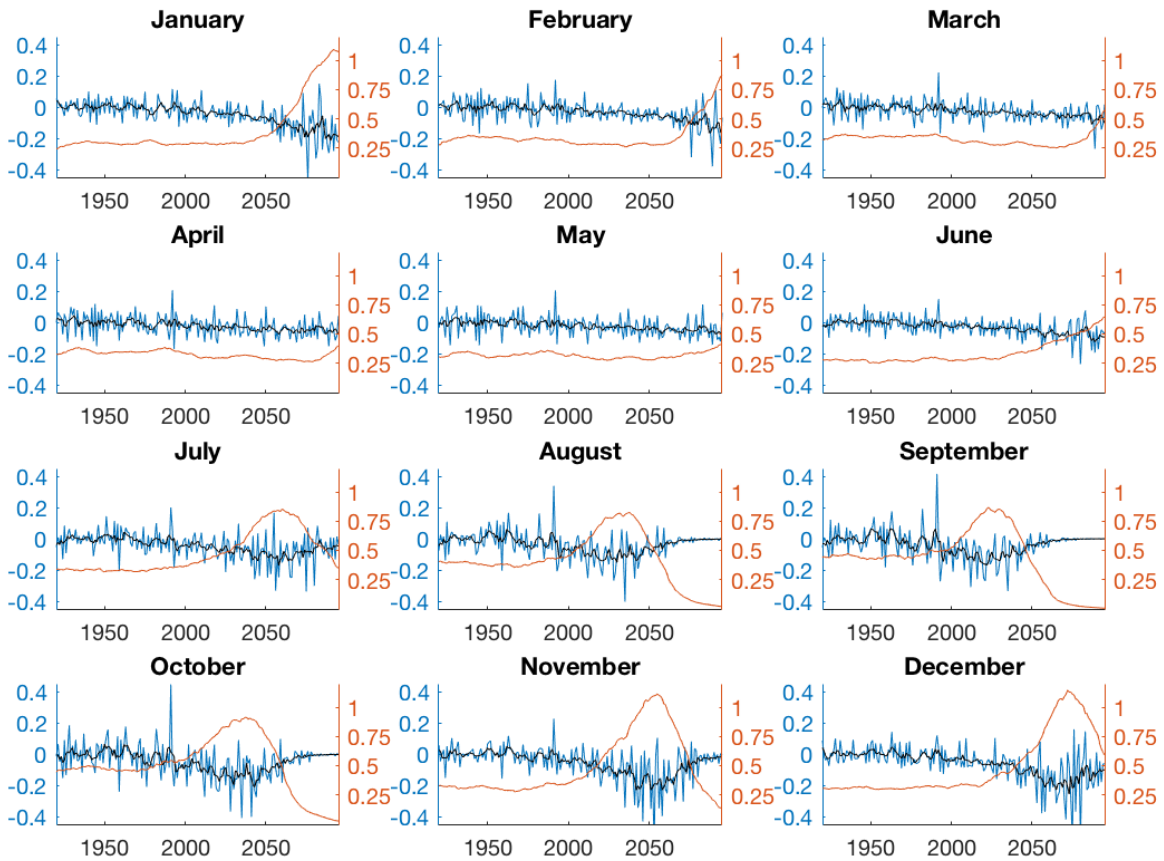


Figure 2: The CESM-LE ensemble mean of the 1-year differences in sea ice area (blue; million km²) with their 5-year running mean overlaid (black) and the running standard deviation of the interannual change in sea ice area (gold; million km²).

641
642
643
644
645
646
647
648
649
650
651
652
653
654
655
656
657
658
659
660
661
662
663
664
665
666
667
668
669
670
671
672
673
674
675
676
677
678

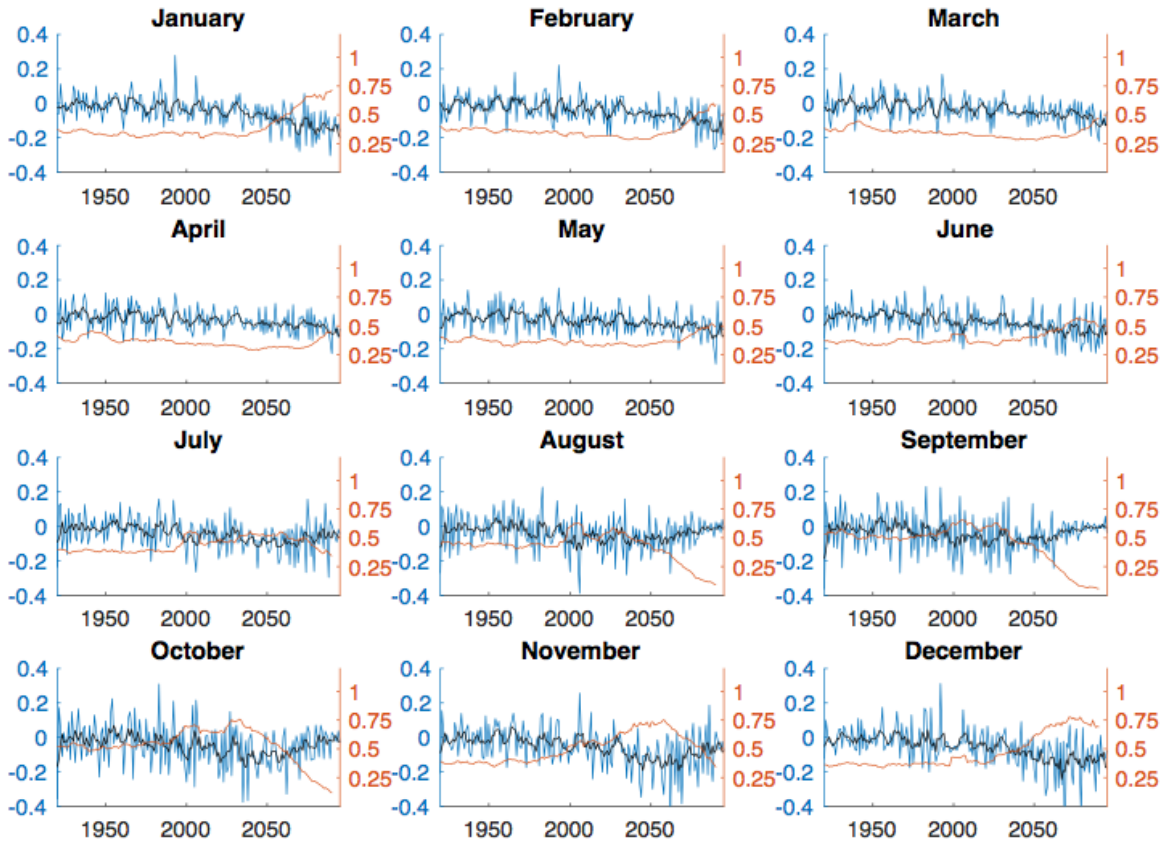
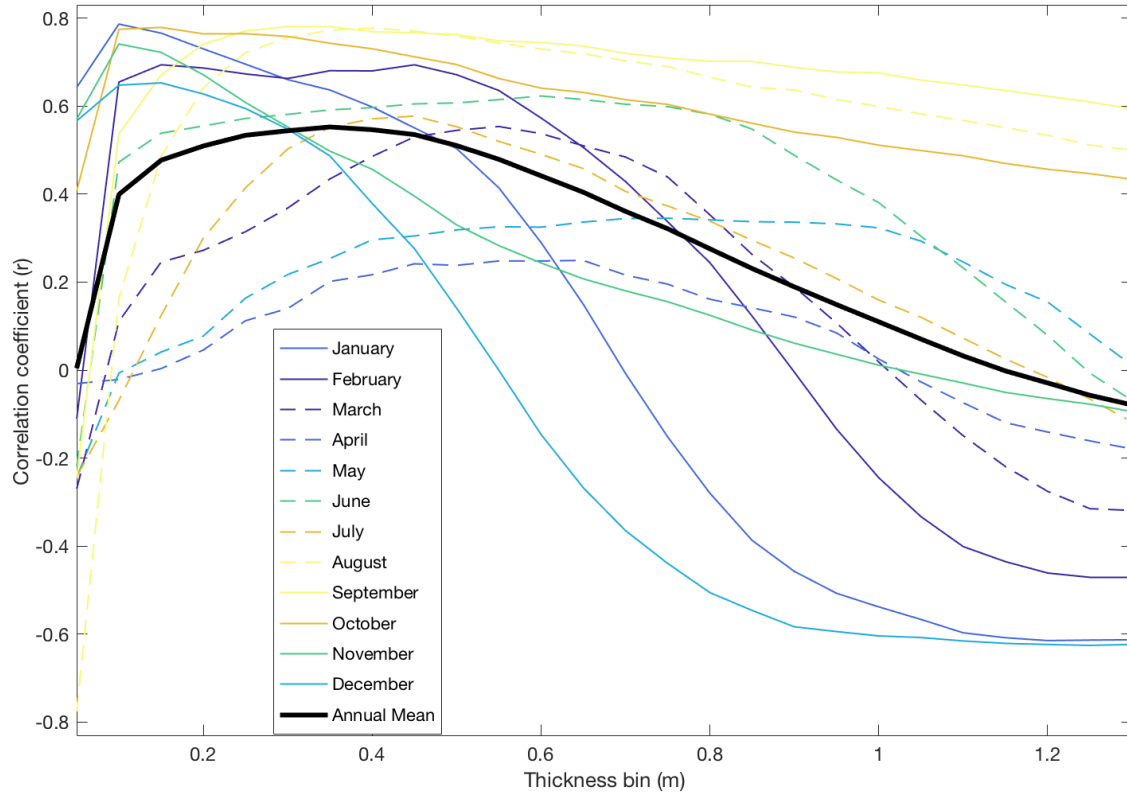


Figure 3: As in Fig. 2, but for the ensemble mean from 12 CMIP5 models' sea ice area.



679 **Figure 4:** Monthly correlation coefficient (r) of the 2000-2100 10-year running standard deviation of 1-year difference in sea ice area with mean grid cell ice thickness binned every 0.05 m of
 680 thickness.
 681
 682
 683

684
685
686
687
688
689
690
691
692
693
694
695
696
697
698
699
700
701
702
703
704
705
706
707
708
709
710
711
712
713
714
715
716
717
718
719
720
721
722
723
724
725
726
727
728

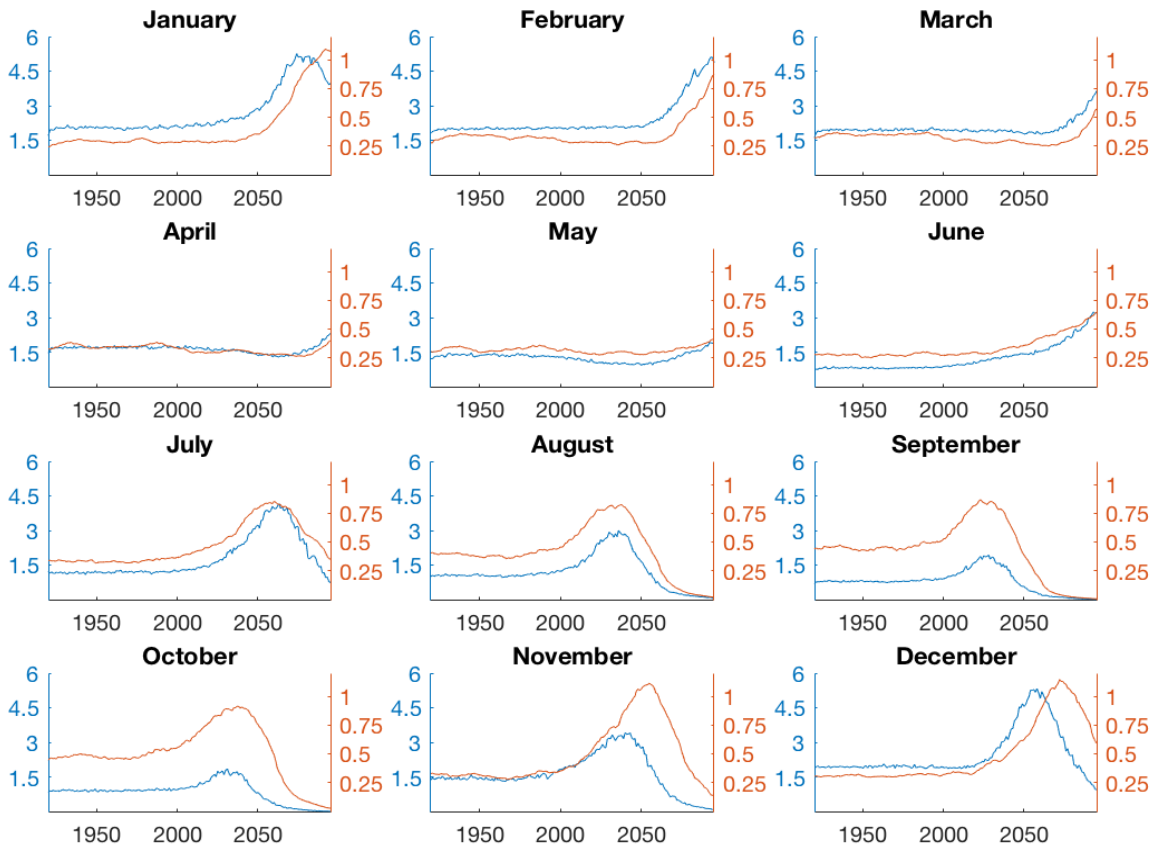
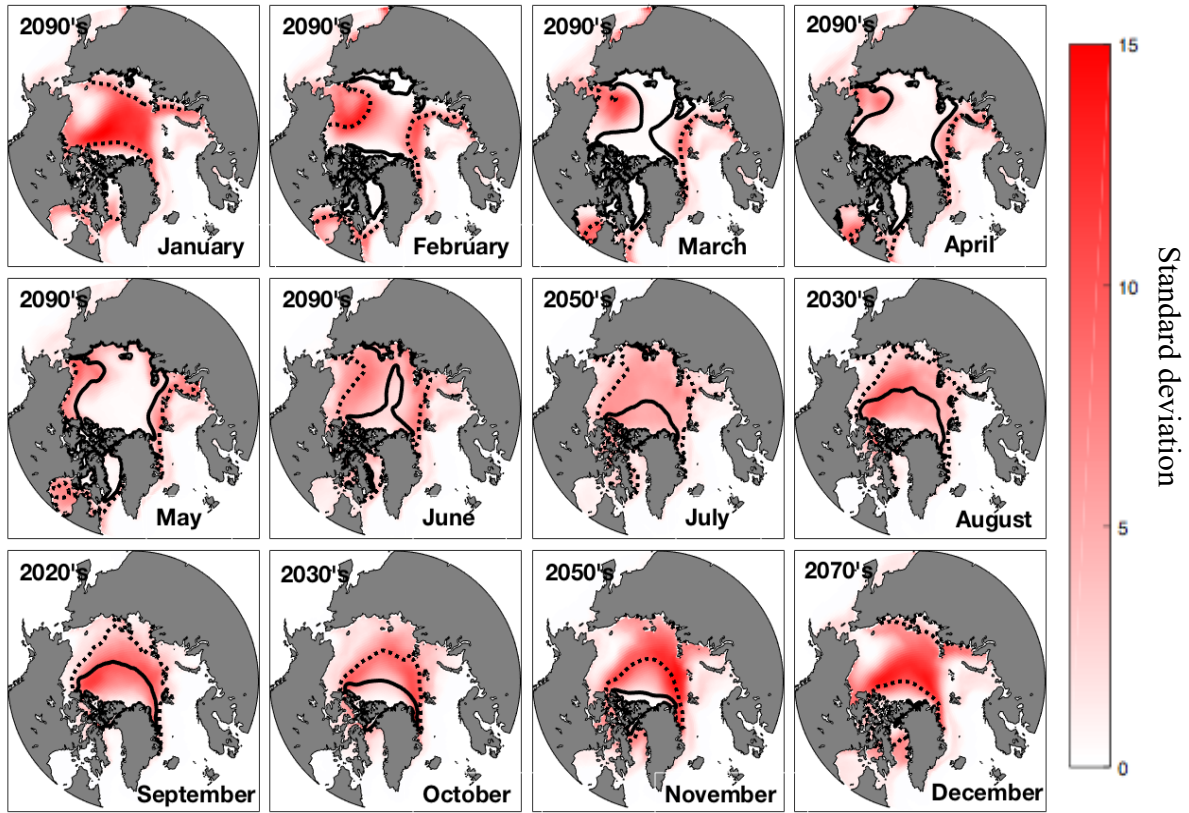


Figure 5: The CESM-LE ensemble mean of the 10-year running standard deviation of 1-year difference in sea ice area from Figure 1 (gold; million km²) and the ensemble mean total area of grid cells with mean ice thickness between 0.2 m and 0.6 m (blue; million km²).

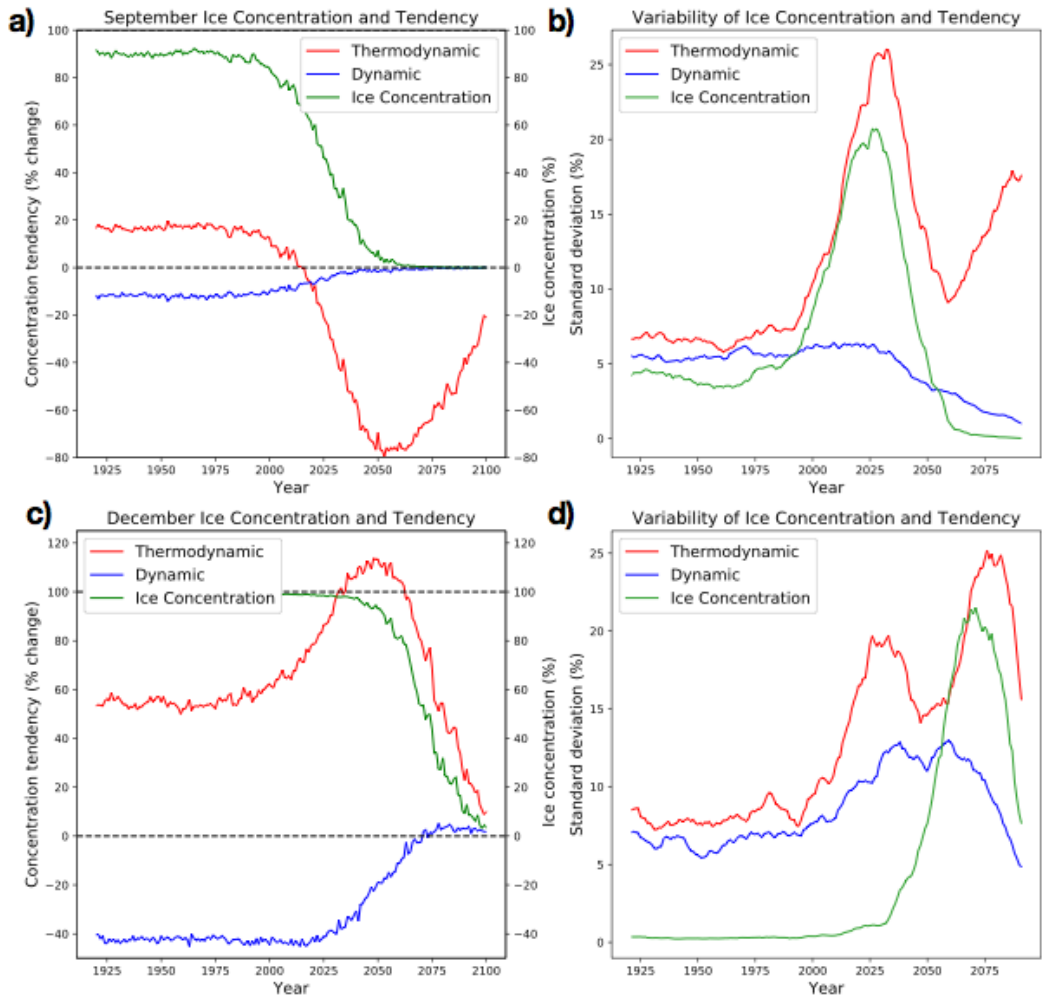
729
730
731
732
733
734



735
736
737
738
739
740
741
742
743
744
745
746
747
748
749
750
751

Figure 6: Monthly ensemble average in CESM-LE of the 10-year running standard deviation of ice concentration (%) in the decade when ice area variability is maximum. Mean 0.2 m and 0.6 m ice thicknesses are indicated by the dotted and solid contours, respectively.

752
753
754
755
756
757



788
789
790
791
792
793
794

Figure 7: Time series of ensemble-mean a) September ice concentration (%) and July-September averaged concentration tendency ($\% \text{ day}^{-1}$) from dynamics and thermodynamics, and b) the 10-year running standard deviation of: the inter-annual difference in ice concentration (%), and July-September ice concentration tendency from dynamics and thermodynamics ($\% \text{ day}^{-1}$). The same information is presented in c) and d) for December concentration and October-December ice concentration tendency terms.

1 Past and future interannual variability of Arctic sea ice in
2 coupled climate models

3
4 John R. Mioduszewski¹, Stephen Vavrus¹, Muyin Wang^{2,3}, Marika [Holland](#)⁴, and Laura [Landrum](#)⁴

5
6
7
8 ¹Nelson Institute Center for Climatic Research, University of Wisconsin—Madison, Madison,
9 Wisconsin.

10 ²Joint Institute for the Study of the Atmosphere and Oceans, University of Washington, Seattle,
11 Washington.

12 ³[Pacific Marine Environmental Laboratory, National Oceanic and Atmospheric Administration,](#)
13 [Seattle, Washington.](#)

14 ⁴[National Center for Atmospheric Research, Boulder, Colorado.](#)

15
16
17
18
19
20
21
22
23
24
25 *Corresponding author: Steve Vavrus, sjvavrus@wisc.edu*
26

Deleted: Future
Formatted: Numbering: Continuous

Deleted: ⁴
Deleted: Holland³
Deleted: Landrum³

Deleted: ¶
Deleted: ³
Deleted: ⁴Pacific Marine Environmental Laboratory, National Oceanic and Atmospheric Administration, Seattle, Washington
Deleted: ¶

Moved (insertion) [2]
Formatted: Font: (Default) Times New Roman

37
38
39
40
41
42
43
44
45
46
47
48
49
50
51
52
53
54
55
56
57
58
59

Abstract

The diminishing Arctic sea ice pack has been widely studied, but mostly focused on time-mean changes in sea ice rather than on short-term variations that also have important physical and societal consequences. In this study we test the hypothesis that future interannual Arctic sea ice area variability will increase by utilizing 40 independent simulations from the Community Earth System Model's Large Ensemble (CESM-LE) for the 1920-2100 period, and augment this with simulations from 12 models participating in the Coupled Model Intercomparison Project Phase 5 (CMIP5). Both CESM-LE and CMIP5 models project that ice area variability will indeed grow substantially, but not monotonically, in every month. There is also a strong seasonal dependence in the magnitude and timing of future variability increases that is robust among CESM ensemble members. The variability in every month is directly correlated with the average ice retreat rate before there is an eventual disappearance in both terms as the ice pack becomes seasonal in summer and autumn by late century. The peak in variability correlates best with the total area of ice between 0.2 - 0.6 m monthly thickness, indicating that substantial future thinning of the ice pack is required before variability maximizes. Within this range, the most favorable thickness for high areal variability depends on the season, especially whether ice growth or ice retreat processes dominate. Thermodynamic melting (top, bottom, lateral) and growth (frazil, congelation) processes are more important than dynamical mechanisms, namely ice export and ridging, in controlling ice area variability.

Moved up [2]: Corresponding author: Steve Vavrus, sjvavrus@wisc.edu

Deleted:

Corresponding author: Steve Vavrus, sjvavrus@wisc.edu

Deleted: a set of

Deleted: ,

Deleted: all

Deleted: s,

Deleted: and with

Deleted: inversely

Deleted: m and

Deleted: primarily due to

Deleted: found to be

87 **1. Introduction**

88
89 Arctic sea ice extent has declined by more than 40% since 1979 during summer (e.g.
90 Stroeve et al. 2012; Serreze and Stroeve 2015; Comiso et al. 2017), primarily as a consequence
91 of greenhouse gas forcing (Notz and Marotzke 2012) but also internal variability (Ding et al.
92 2017). While this trend is greatest in summer, substantial losses are observed throughout the year
93 (Cavalieri and Parkinson 2012) resulting in an ice season duration that is up to 3 months shorter
94 in some regions (Stammerjohn et al. 2012). Reduced ice area is accompanied by a greater frac-
95 tion of younger ice (Nghiem et al. 2006; Maslanik et al. 2007a, 2011), which reduces the mean
96 thickness of the basin ice pack (Kwok and Rothrock 2009; Kwok et al. 2009; Lang et al. 2017).
97 As a result, the estimated negative trend in sea ice volume (-27.9% per decade) is about twice as
98 large as the trend in sea ice area (-14.2% per decade; Overland and Wang 2013).

100 Output from many climate models suggests that the Arctic sea ice cover will not retreat in
101 a steady manner, but will likely fluctuate more as it diminishes, punctuated by occasional Rapid
102 Ice Loss Events (RILEs; Holland et al. 2006; Döscher and Koenigk 2013). The overall decline in
103 ice cover is expected to continue (Collins et al. 2013), and the Arctic may become seasonally ice-
104 free within a few decades, depending on emissions pathway (Stroeve et al. 2007; Wang and
105 Overland 2009; 2012; Massonnet et al. 2012; Wang and Overland 2012; Overland and Wang
106 2013; Jahn et al. 2016; Notz and Stroeve 2016). However, internal variability confounds predic-
107 tion of this timing (Stocker et al. 2013; Swart et al. 2015; Jahn et al. 2016; Labe et al. 2018), and
108 even the definition of ice-free differs among Arctic stakeholders (Ridley et al. 2016). Nonethe-
109 less, navigation through the Arctic has already increased in frequency as a result of this decline
110 (Melia 2016; Eguíluz et al. 2016), and even more trade routes associated with the increased ice-
111 free season are expected by the end of the 21st century (Aksenov et al. 2015; Stephenson and
112 Smith 2013).

114 As the Arctic sea ice pack thins and retreats, multi-year ice is being lost and there is con-
115 sequently a larger proportion of seasonal, thin first-year ice (Kwok et al., 2010; Maykut 1978;
116 Holland et al. 2006). Overall thinner ice may result in an ice pack that exhibits greater inter-
117 annual variability (Maslanik et al. 2007b; Goosse et al. 2009; Notz 2009; Kay et al. 2011; Hol-
118 land and Stroeve 2011; Döscher and Koenigk 2013), at least partially due to enhanced ice growth
119 and melt (Maykut 1978; Holland et al. 2006; Bathiany et al. 2016a). Decreased ice thickness
120 promotes amplification of a positive ice-albedo feedback, which can magnify sea ice anomalies
121 (Perovich et al. 2007), and thin ice is more vulnerable to anomalous atmospheric forcing and
122 oceanic transport due to the smaller amount of energy required to completely melt the ice
123 (Maslanik et al. 1996, Zhao et al. 2018). For example, pulse-like increases in oceanic heat
124 transport can trigger abrupt ice-loss events in sufficiently thin ice (Woodgate et al. 2012).

126 Changes in the interannual variability of sea ice have been studied only in a limited ca-
127 pacity, likely because they are only beginning to become visible in September in the present day.
128 Both Goosse et al. (2009) and Swart et al. (2015; their Fig. S6) reported that maximum ice area
129 variability during September occurs once the mean ice extent declines to 3-4 million km². This
130 increased variability may occur due to increased prevalence of RILEs and periods of rapid re-
131 covery during this timeframe (Döscher and Koenigk 2013). The thickness distribution during
132 these periods skews toward thinner ice, which is conducive to both rapid ice loss and rapid re-

Deleted: ¶

- Deleted: mean
- Deleted: Many
- Deleted: s
- Deleted: will likely

- Deleted: with
- Deleted: a substantial
- Deleted: opening of

- Deleted: reduces
- Deleted: in extent
- Deleted: Increased thin

- Deleted: retreat rates

- Deleted: The relationship between
- Deleted: sea ice are
- Deleted: a
- Deleted: and its variability
- Deleted: s
- Deleted: it
- Deleted: is
- Deleted: sea

172 recovery processes (Tietsche et al. 2011; Döscher and Koenigk 2013). Holland et al. (2008) con-
173 sidered a critical ice thickness that can serve as a precursor to RILEs, but found it more likely
174 that intrinsic variability played the primary role in the particular RILEs that were studied. More
175 recently, Massonnet et al. (2018) analyzed the projected variability of sea ice volume and its pro-
176 jected future change in the CMIP5 ensemble, which suggested a monotonic future decrease. The
177 corresponding variability of sea ice area was investigated by Olonscheck and Notz (2017), but
178 their analysis was much coarser temporally and seasonally, in that it only compared changes be-
179 tween entire blocks of time (the historical 1850-2005 period vs. the future 2006-2100 interval)
180 and was further restricted to the summer and winter seasons.

181
182 Building on these previous studies, our paper has two novel aspects. First, we analyze the
183 transient interannual variability of sea ice area over the course of the year from the early 20th
184 century through the entire 21st century and find very different behavior across the four seasons.
185 These monthly differences are societally important, because marine access to the Arctic will like-
186 ly expand beyond late summer as the ice pack shrinks. Second, we detail how interannual sea ice
187 area variability changes as the ice pack retreats, and we link enhanced future variability to opti-
188 mal ice thicknesses and to the various thermodynamic and dynamic processes that control ice
189 area variability. We analyze a large 40-member ensemble from a single GCM, which allows us
190 to isolate internal variability, which is otherwise muddled with inter-model variability in multi-
191 model comparisons. This allows us to test the hypothesis that inter-annual Arctic sea ice cover
192 variability will increase throughout the year in the future as the ice pack diminishes.

Deleted: that have focused primarily on variability at the summer ice minimum

Deleted: through

Deleted: the

Deleted: for our study

Deleted: has the advantage of

Deleted: allowing us to robustly characterize

195 2. Data and Methods

196
197 Ice thickness, concentration, and area were obtained from simulations of the Community
198 Earth System Model Large Ensemble Project (CESM-LE). Ice concentration refers to the per-
199 centage of a given grid cell that is covered by ice, while ice area in this study refers specifically
200 to this percent coverage multiplied by the area of the grid cell yielding a total Arctic ice-covered
201 area. The CESM-LE was designed to enable an assessment of projected change in the climate
202 system while incorporating a wide range of internal climate variability (Kay et al. 2015). It con-
203 sists of 40 ensemble members simulating the period 1920-2100 under historical and projected
204 (RCP8.5 emissions scenario only) external forcing. The ensemble members are produced by in-
205 troducing a small, random round-off level difference in the initial air temperature field for each
206 member. This then generates a consequent ensemble spread that is purely due to simulated inter-
207 nal climate variability. A full description of the CESM-LE is given in Kay et al. (2015), and sim-
208 ilar ensembles using the weaker RCP4.5 and RCP2.6 scenarios can be found in Sanderson et al.
209 (2017, 2018).

210
211 Another data set used in the current study is the model simulations from the Coupled
212 Model Intercomparison Project Phase 5 (CMIP5). Although more than 40 models submitted their
213 simulation results to the Program for Climate Model Diagnosis and Intercomparison (PCMDI),
214 only 12 of them simulated the Arctic sea ice extent both of the monthly means (each individual
215 month) and the magnitude of the seasonal cycle (March minus September sea-ice extent) within
216 20-percent error when compared with observations (Wang and Overland, 2012, Wang and Over-
217 land 2015). Therefore, we used only these 12 models identified by Wang and Overland (2015) in

225 this study; ACCESS1.0, ACCESS1.3, CCSM4, CESM1(CAM5.1), EC-EARTH, HadGEM2-
 226 AO, HadGEM2-CC, HadGEM2-ES, MIROC-ESM, MIROC-ESM-CHEM, MPI-ESM-LR, and
 227 MPI-ESM-MR. Among the 12 models, half of them use the same sea ice model as CESM-LE
 228 (CICE, Hunke and Lipscomb 2010) or a variation of it. If a GCM provided multiple ensemble
 229 members, we only kept up to 5 realizations, so that the total ensemble numbers is close to that
 230 used in CESM-LE. There are a total of 33 ensemble members from these 12 models in the
 231 RCP8.5 emissions scenario. Sea ice area, rather than ice extent, is computed from these 12
 232 CMIP5 models to be consistent with CESM-LE results.

233
 234 One of our primary analysis datasets is the time series of monthly ice variables. The en-
 235 semble mean of all variables is taken after the statistics are calculated for each ensemble mem-
 236 ber. 1-year differences in ice area are calculated for each month separately to remove the con-
 237 founding effect of amplified variability resulting from a downward trend. Finally, a 10-year run-
 238 ning standard deviation is applied to the time series of 1-year differences in monthly ice area,
 239 centered on a given year. Ten years was chosen to quantify variability over decadal-scale inter-
 240 vals and to provide an adequate number of years for a standard deviation calculation. The timing
 241 and magnitude of variability is generally insensitive to the standard deviation window, however,
 242 and whether the 1-year difference in ice area or its raw time series is used.

245 3. Results

247 3.1 Sea ice area and its variability

249 Sea ice area in the CESM-LE is projected to decline in all months in the 21st century,
 250 proceeding in three phases: a fairly stable regime of extensive coverage in the 20th century, then
 251 a decline, followed by virtually no ice remaining in summer and autumn months (Fig. 1). Sea ice
 252 area variability follows an analogous three-phase progression in months spanning mid-summer
 253 to early winter (Fig. 2). For example, in September this includes a period of modest variability
 254 during the 20th century, then a distinct variability peak in the late 2020s and 2030s that coincides
 255 with the maximum rate of ice retreat, and finally negligible variability in the late 21st century as
 256 the Arctic reaches near ice-free conditions (Fig. 2). The first two phases of this progression in
 257 variability occur for months in late winter to early summer (January-June), and suppressed varia-
 258 bility would likely emerge beyond the end of the century, assuming that ice cover in these
 259 months would continue to retreat. The maximum rate of ice retreat (negative values of the de-
 260 rivative) occurs at a different time in the 21st century in each month, occurring presently in Sep-
 261 tember but not until the end of the century in spring.

263 The same relationship between ice area and its variability is maintained across CMIP5
 264 models, though with more noise resulting from the aggregation of many different models rather
 265 than ensemble members from a single model (Fig. 3). This is most notable in the sea ice area (1-
 266 year difference) time series (Fig. 3, blue), indicating that there is considerable spread in when
 267 and how the downward trend proceeds each month, as found in Massonnet et al. (2012), but
 268 good agreement that variability increases in this timeframe.

Deleted: . The 12 models are

Deleted: are using CICE (?need the name) or a variation of CICE as their sea-ice model component

Deleted: When model has more ensemble members provided, we only kept up to 5 ensemble members from each model so that the total ensemble numbers are close to the CESM-LE

Deleted: ;

Deleted: there are 33

Deleted: obtained

Deleted: statistics

Deleted: <object>

Formatted: Font: (Default) Times New Roman, 12 pt

Deleted: ¶

Figure 1: The CESM-LE ensemble mean time series of monthly sea ice area (km² x 10⁶). ¶

... [1]

Moved down [1]: Figure 1: The CESM-LE ensemble monthly sea ice area (km² x 10⁶). ¶

Formatted: Font: (Default) Times New Roman, 12 pt

Deleted: S1

Deleted:

Deleted: also

Deleted: this

Deleted: 1

Deleted: 1

Deleted: ¶

... [2]

Formatted: Font: (Default) Times New Roman, 12 pt

Deleted: inverse

Deleted: 2

Deleted: 2

The analysis of ice area variability in Fig. 2 and Fig. 3 follows that of Goosse et al. (2009) and Swart et al. (2015), but we extend their findings for September to all months and confirm that the variability in ice area is maximized as its total basin area decline is well underway in both CESM-LE ensembles and across CMIP5 models. A direct relationship between the rate of sea ice retreat and the magnitude of variability is present across all months in CESM-LE and CMIP5: the standard deviation is highest when ice declines the fastest (Figs. 1 and 2). Furthermore, the magnitude and timing of peak ice area variability in both sets of experiments differs greatly by season. The peak in magnitude in CESM-LE is most pronounced from November–January when the running standard deviation of ice area exceeds 1×10^6 km², while the lowest magnitudes occur in April and May, when the downward trend in ice area does not peak prior to 2100 (Fig. 2). Near the end of the 21st century, the running standard deviation also shows an increase in the CMIP5 ensembles from December to June (Fig. 3), very similar behavior to that displayed by CESM-LE. However the magnitude of the increase in the running standard deviation in the CMIP5 ensemble mean is smaller than that in CESM-LE. This is not surprising, as the timing of ice retreat varies among models, so averaging them will smooth out the possible signals. The CMIP5 models therefore provide additional evidence that increased variability is associated with decreasing sea ice cover.

3.2 Relationship between ice area variability and thickness

Because increasing future concentrations of thin ice are likely a primary factor in increased ice area variability, we next consider the relationship between ice thickness and ice area variability in CESM-LE. This is done by correlating the standard deviation of basin-wide ice area (Fig. 2) with the total area of grid cells with mean ice thickness within a given range for an aggregation of all years and ensemble members, binned at 0.05 m intervals (Fig. 4). 20th century data are omitted because both variables are largely stationary for this period. There is a large difference in the maximum correlation coefficient across seasons, but in most months it peaks between $r = 0.6$ and $r = 0.8$. This peak is associated with the thinnest ice of 0.1 m to 0.2 m from October to January. There is a broad peak in the correlation coefficient between 0.25 m and 0.40 m in August and September, while July peaks near 0.45 m thickness but with a weaker maximum correlation coefficient ($r = 0.6$). In June, $r = 0.6$ for most ice thicknesses below 0.8 m, and there is only a weak correlation between these variables in April and May.

The analysis in Fig. 4 allows us to identify a common range of ice thicknesses when ice area variability generally peaks regardless of the month, which we approximate as 0.2 m to 0.6 m. We next track the temporal evolution of this thin ice throughout the basin by calculating the total area of ice that falls within that range. The time-transgressive nature of when the peak in thin ice cover occurs (earliest in September, latest in winter-spring) is consistent with the corresponding timing of the peak future sea ice area variability, suggesting that the emergence of a sufficiently thin and contracted ice pack is a primary factor for enhanced ice cover variability (Fig. 5). Both curves match each other in shape, with a steady state early, increasing to a peak and dropping to zero as the Arctic becomes ice-free. The exception is in the spring and early summer when neither increases until the end of the 21st century, when ice begins to decline more rapidly. The two curves are largely in phase as well, with one preceding the other by no more than 10–20 years in July, August, and November–January. The phase difference is due to the

Deleted: l and Fig. 32...follows that of Goosse et al... [3]

Deleted: n invers

Deleted: e relationship between the rate of sea ice retreat [4]

Formatted: Font color: Auto

Deleted: shown b

Deleted: y

Deleted: is different in different...aries among models... [5]

Deleted: Part of this

Deleted: the ...increased variability ... [6]

Deleted: r, but the CMIP5 model spread could also be responsible for inflated variance as models diverge in their [7]

Deleted: Figure 43: Monthly correlation coefficient (r) of the 2000–2100 10-year running standard deviation of 1-yr [8]

Deleted: <object>

Formatted: Font: (Default) Times New Roman, 14 pt, Bold

Deleted: its

Deleted: l) with the total area of grid cells with mean ice [9]

Deleted: 1) with the total area of grid cells with mean ice [9]

Deleted: 1) with the total area of grid cells with mean ice [9]

Deleted: 1) with the total area of grid cells with mean ice [9]

Deleted: 1) with the total area of grid cells with mean ice [9]

Deleted: 1) with the total area of grid cells with mean ice [9]

Deleted: 1) with the total area of grid cells with mean ice [9]

Deleted: 1) with the total area of grid cells with mean ice [9]

Deleted: 1) with the total area of grid cells with mean ice [9]

Deleted: 1) with the total area of grid cells with mean ice [9]

Deleted: 1) with the total area of grid cells with mean ice [9]

Deleted: 1) with the total area of grid cells with mean ice [9]

Deleted: 1) with the total area of grid cells with mean ice [9]

Deleted: 1) with the total area of grid cells with mean ice [9]

Deleted: 1) with the total area of grid cells with mean ice [9]

Deleted: 1) with the total area of grid cells with mean ice [9]

Deleted: 1) with the total area of grid cells with mean ice [9]

Deleted: 1) with the total area of grid cells with mean ice [9]

Deleted: 1) with the total area of grid cells with mean ice [9]

Deleted: 1) with the total area of grid cells with mean ice [9]

Deleted: 1) with the total area of grid cells with mean ice [9]

Deleted: 1) with the total area of grid cells with mean ice [9]

Deleted: 1) with the total area of grid cells with mean ice [9]

Formatted: Font: (Default) Times New Roman, 12 pt, Underline color: Red, Font color: Red

Deleted: 3 allows us to identify a common range of ice [11]

Deleted: 3 allows us to identify a common range of ice [11]

Deleted: 3 allows us to identify a common range of ice [11]

Deleted: 3 allows us to identify a common range of ice [11]

Deleted: 3 allows us to identify a common range of ice [11]

Deleted: 3 allows us to identify a common range of ice [11]

Deleted: 3 allows us to identify a common range of ice [11]

Deleted: 3 allows us to identify a common range of ice [11]

Deleted: 3 allows us to identify a common range of ice [11]

Deleted: 3 allows us to identify a common range of ice [11]

Deleted: 3 allows us to identify a common range of ice [11]

Deleted: 3 allows us to identify a common range of ice [11]

Deleted: 3 allows us to identify a common range of ice [11]

438 chosen range of ice thicknesses, since the best relationship varies by month (Fig. 4). The two
439 curves are in phase from August-October (Fig. 5) when the 0.2 m to 0.6 m range approximates
440 the best relationship between thickness and variability (Fig. 4). However, ice area variability
441 maximizes after the peak in 0.2 m – 0.6 m thickness area in November–January, because varia-
442 bility is more highly correlated with ice slightly thinner than 0.2 m in these months (Fig. 4; Fig.
443 5).

445 There are also notable seasonal differences in the spatial pattern of variability during the
446 decade when variability in ice concentration peaks in CESM-LE (Fig. 6). The largest fluctuations
447 occur in a horseshoe-shaped pattern across the Arctic Ocean in autumn, but they are restricted to
448 the boundaries of the Atlantic and Pacific Oceans in late winter and spring. The result is a larger
449 area of high variability in the second half of the year and into January. The mean 0.2 m (dotted)
450 and 0.6 m (solid) ice thickness contours are overlaid for reference (Fig. 6). The contours corre-
451 spond closely to the boundary of maximum variability in ice coverage in most months, which is
452 consistent with results from Fig. 4 and Fig. 5. This demonstrates the first-order relationship be-
453 tween thin ice and the variability of inter-annual ice coverage within a given region.

455 3.3 Ice concentration tendency

456 The strong relationship between thin ice coverage and high concentration variability oc-
457 curs primarily due to the differing underlying mechanisms controlling ice concentration variabil-
458 ity at a given time, namely whether ice is expanding or retreating. To illustrate this, we chose
459 two months representative of these processes, September and December, to conduct an in-depth
460 analysis of the physical mechanisms involved in the time difference in the two curves in Fig. 5.
461 September is the end of the melt season, and therefore the ice concentration over the entire basin
462 in this month reflects the cumulative impact of melt processes throughout the summer. By con-
463 trast, December is a time of ice growth, particularly in the future, and thus the ice concentration
464 in this month is largely regulated by cumulative growth processes during the autumn. Using
465 available model output, we calculate the ice concentration tendency (% day⁻¹) from thermody-
466 namics and dynamics in the regions where the decadal standard deviation of ice concentration
467 exceeds 30% within the grid cell (Fig. S1) to evaluate the mean ice budget. These regions of
468 maximum variability in September and December closely match those in Fig. 6, though the mag-
469 nitude is smaller in Fig. 6 due to the standard deviation being a decadal mean. The daily change
470 in ice concentration is a function of dynamic contributions (ice import/export and ridging), ther-
471 modynamic melt processes (the sum of top, basal, and lateral), and thermodynamic growth (frazil
472 and congelation). Because antecedent conditions of the icepack can be an important factor for
473 determining ice concentration in the month of interest, we sum these terms over the preceding
474 months (July-September or October-December) and report the net 3-month change in ice concen-
475 tration resulting from each component.

476
477
478 The most interannually variable ice cover during September occurs primarily in the 2020s
479 and is centered across the central Arctic (Fig. S1a), though this region displays net ice expansion
480 in July-September in the 20th century (Fig. 7a) due to rapid ice growth in September. Thermo-
481 dynamic processes dominate over dynamics and are of opposing sign during the 20th century,
482 and thermodynamic processes add an average of 20% to the ice concentration of each grid cell in
483 the region by the end of September, compared with a loss of only 10% from dynamical processes

Deleted: 3

Deleted: 4

Deleted: 3

Deleted: <object>

Formatted: Font: (Default) Times New Roman, 12 pt

Deleted: 3

Deleted: 4

Deleted: ¶

Figure 65: Monthly ensemble average in CESM-LE of the 10-year running standard deviation of ice concentration (%) in the decade when ice area variability is maximum. Mean 0.2 m and 0.6 m ice thicknesses are indicated by the dotted and solid contours, respectively. ¶

Deleted: 5

Deleted: 5

Deleted: 3

Deleted: 4

Deleted: <object>

Formatted: Font: (Default) Times New Roman, 12 pt

Deleted: growing

Deleted: 4

Deleted: 2

Deleted: 5

Deleted: 5

Deleted: a slightly different method of calculating the standard deviation

Deleted: 2

Deleted: 6

511 (Fig. 7a). Ice growth diminishes and melt processes accelerate in the early-mid 21st century
512 when the melt processes reduce ice concentration by more than 75% and the dynamic processes
513 essentially disappear with less ice to export (Fig. 7a). After 2060, September ice-free conditions
514 occur, and the thermodynamic term becomes less negative due to reduced areal coverage of ice
515 in June and hence less ice area to melt over the summer (Fig. 7a).

516
517 Because thermodynamic processes dominate in controlling ice concentration in the fu-
518 ture, they should also be the first-order forcing explaining future ice concentration variability,
519 particularly given that the magnitude of the dynamic contribution approaches zero by the 2020s
520 when ice cover is rapidly diminishing. As shown in Figure 7b, the peak interannual variability in
521 the thermodynamic term (red curve) is indeed several times larger than peak variability of the
522 dynamic term (blue curve), and the variability in the thermodynamic term maximizes during the
523 late 2020s in phase with the variability of the ice concentration (green curve) when the thermo-
524 dynamic term is declining most rapidly in Figure 7a. The variability likely also reflects the influ-
525 ence of the surface albedo feedback in amplifying summer ice area variations. There is a second-
526 ary rise in the variability of the thermodynamic term after 2060 (Figure 7b), coinciding with its
527 rapid rise toward zero in Figure 7a, but ice coverage by this point is confined to a diminishing
528 area.

529
530 From the 20th century well into the 21st century, ice growth occurs in the October-
531 December period in a similar region of maximum interannual variability as September, except
532 slightly equatorward (Fig. S1b). Ice export plays a relatively larger role in the regions of interest
533 in December than in September (Fig. 7c). However, the thermodynamic tendency is still the
534 dominant term controlling ice concentration within this region of maximum interannual variabil-
535 ity, and this term increases in the early-mid 21st century to a total of nearly 120%, some of which
536 is offset by ice export that contributes to a 40% decrease in mean ice concentration in the 20th
537 and early 21st centuries (Fig. 7c). The increased net ice growth occurs at this time primarily be-
538 cause there is more initial open water on which frazil ice can form.

539
540 Figure 7d shows that the standard deviation of December ice concentration (green curve)
541 peaks around 2070 and is accompanied by a peak in the variability of the thermodynamic ten-
542 dency (red curve) of more than double the magnitude of its dynamic tendency (blue curve). A
543 smaller first peak in thermodynamic tendency occurs in the 2020s, when ice growth in this re-
544 gion increases due to increased frazil growth as this region's waters become more open on aver-
545 age in October. This initial peak may be smaller due to the anti-correlation between dynamic and
546 thermodynamic tendency, which reduces the effect of the latter. The rapid subsequent decline in
547 ice growth occurs as conditions become too warm for ice growth over much of the October-
548 December period in the 2050s and 2060s (Fig. 7c). This is reflected in the peak in variability of
549 the thermodynamic tendency (red curve) approximately corresponding to the timing of the peak
550 in the ice area variability (green curve) in 2070 (Fig. 7d). The coincidence in their peak variabil-
551 ity is similar to that in Figure 7b and underscores the dominance of thermodynamics over dy-
552 namics in regulating the variability of ice area.

553 4. Discussion and Conclusions

554
555
556

Deleted: 6

Deleted: 6

Deleted:

Deleted: 6

Deleted: Figure 76: Time series of ensemble-mean a) September ice concentration (%) and July-September averaged concentration tendency (% day⁻¹) from dynamics and thermodynamics, and b) the 10-year running standard deviation of: the inter-annual difference in ice concentration (%), and July-September ice concentration tendency from dynamics and thermodynamics (% day⁻¹). The same information is presented in c) and d) for December concentration and October-December ice concentration tendency terms.

Deleted: ¶

Deleted: 6

Deleted: thermodynamic

Deleted: 6

Deleted: thermodynamic term

Deleted: 6

Deleted: 6

Deleted: Ice

Deleted: rather than melt

Deleted: 2

Deleted:),

Deleted: from the 20th century well into the 21st century, anice

Deleted: 6

Deleted: 6

Deleted: ¶

¶
Figure 6: Time series of ensemble-mean a) September ice concentration (%) and July-September averaged concentration tendency (% day⁻¹) from dynamics and thermodynamics, and b) the 10-year running standard deviation of: the inter-annual difference in ice concentration (%), and July-September ice concentration tendency from dynamics and thermodynamics (% day⁻¹). The same information is presented in c) and d) for December concentration and October-December ice concentration tendency terms.¶

Deleted: ¶

Deleted: 6

Deleted: 6

Deleted: 6

Deleted: 6

602 This study has assessed the behavior of interannual Arctic sea ice area variability in the
603 past and future, using a large set of independent realizations from the CESM-LE and simulations
604 from 12 models participating in CMIP5. The results demonstrate the complex, time-varying re-
605 sponse of the ice pack as it transitions from a relatively stable state during the 20th century to a
606 more volatile one. A few of our most important findings are summarized below.

607
608 1) Inter-annual variability of Arctic sea ice cover increases (at least transiently) in all
609 months in the future as sea ice area and thickness decline, but there is a strong seasonal depend-
610 ence. There is also a strong seasonal dependence of the magnitude of the maximum ice area vari-
611 ability in the future, with the greatest magnitude occurring during autumn and winter and small-
612 est during spring by the time the simulation ends in 2100 (Fig. 2-3). The future peak in variabil-
613 ity emerges soonest in late-summer months and latest during spring months, and the magnitude
614 of this peak is positively correlated with the rate of ice loss in every month.

615
616 It is possible that the seasonal differences in ice area variability are partially a construction
617 of the geography of the Arctic Basin, as evident in Fig. 6; when the ice margin is geographically
618 constrained and unable to expand and contract due to a coastline early in the simulation, there is
619 a smaller area subject to high ice variability. This explanation was offered by Goosse et al.
620 (2009) for the same relationship in summer ice area variability, as well as by Eisenman (2010) to
621 explain retreat rate differences between summer and winter. In the future, the ice in the central
622 Arctic Ocean becomes thin enough to expand and contract extensively each season, leading to an
623 increase in variability. Therefore, variability could be considered to be limited particularly in the
624 first phase of its time series (Fig. 2) by the inability of ice to spread across a large open area.
625 Support for this interpretation comes from our calculation of Eisenman's equivalent ice area ap-
626 plied to Fig. 1 (not shown), which resulted in the largest absolute decline in sea ice during the
627 winter-spring months, though summer-autumn ice loss was still greater in relative terms. While
628 useful for approximating potential sea ice extent in the absence of geographic constraints, equiv-
629 alent ice area is still a theoretical construct; our purpose is to assess the variability of ice cover
630 that actually exists. Furthermore, results from Fig. 4 and Fig. 5 suggest that the amount of thin
631 ice alone can explain the evolution of ice variability in every month, though differences in the
632 optimal ice thickness by month may require a partial geographical explanation in addition to one
633 incorporating the components of the thermodynamic tendency of ice area from Fig. 7.

634
635 2) Ice needs to be sufficiently thin before areal variability maximizes, and in CESM-LE the
636 optimal thickness range is generally between 0.2 m to 0.6 m but with some seasonal dependence
637 resulting from the ice melt or ice growth processes that dominate in a given season (Fig. 4-5).
638 The mean ice thickness in late summer and autumn is close to 0.6 m when ice area variability is
639 highest, but is 0.2 m or less for a grid cell average in the winter.

640
641 Increased ice area variability in summer and fall is partly attributable to a higher efficien-
642 cy of open water formation with the thinning sea ice (Holland et al., 2006) and the fact that
643 smaller heating anomalies are required to completely melt through vast areas of the thin ice pack
644 (Bitz and Roe, 2004). We find that the total area of thin ice between the range 0.2 m to 0.6 m is
645 closely related to how soon and how strongly the peak variability in basin-wide ice area emerges,
646 and this is primarily a function of variability in ice area's thermodynamic tendency. This is con-
647 sistent with a physical understanding of this relationship, since ice that is too thin tends to be sea-
648 sonal and melt off every year, whereas thick ice is more likely to survive the melt season. Sea-

Deleted: 1,2

Deleted: ¶

Deleted: inversely

Deleted: 5

Deleted: Our calculation of equivalent ice area applied to Fig. 1 (not shown) resulted in the expected larger drop in sea ice during the winter-spring months which result in greater peaks in their variability, though autumn and winter ice loss and variability were still greater. However, equivalent ice area is a theoretical construct and our purpose is to assess the variability of ice cover that actually exists.

Deleted: However, i

Deleted: 1

Deleted: 3

Deleted: 4

Deleted: 6

Deleted: 3

666 sonal forecasting of September sea ice coverage takes advantage of this concept, with the fore-
667 cast skill improved when initializing ice thickness up to 8 months in advance (Chevallier et al.,
668 2012; Day et al., 2014).

669
670 In contrast, ice area variability in November-January arises primarily from inter-annual
671 variability in ice growth (as represented by December in Fig. 7c,d), which is dependent on exist-
672 ing open water conditions and temperature anomalies. The peak in ice area variability in these
673 months also coincides with a slightly lower mean ice thickness of 0.2 m, though it is unclear
674 whether that is due to these ice growth rather than melt processes at work during the winter.
675

676 3) Interannual variability in ice concentration is driven primarily by thermodynamic mecha-
677 nisms, which are primarily comprised of either ice growth or ice melt depending on the season.
678 Despite being opposing processes, their magnitudes exceed those of dynamic ice processes (Fig.
679 7).

680
681 The thermodynamic tendency in ice concentration is of much greater magnitude than its
682 dynamic counterpart at both the end of the melt season and start of the growth season, and the
683 maximum interannual variability of the thermodynamic term is mostly in phase with that of ice
684 concentration. The inverse relationship between ice area's interannual variability and its interan-
685 nual rate of change (Figs. 1 and 2) is also found between the thermodynamic tendency and its
686 rate of change (not shown, but inferred from Fig. 7). This is further evidence that ice area varia-
687 bility is primarily driven by thermodynamic processes in the icepack.
688

689 The dominance of the thermodynamic tendency is unsurprising and has been established as
690 the relatively more important set of processes controlling sea ice variability, primarily via
691 transport of mid-latitude eddy heat flux anomalies (Kelleher and Screen, 2018), anticyclone pas-
692 sage (Wernli and Lukas, 2018), and increased ocean heat transport (Li et al., 2018). However,
693 the dynamic contribution to changes in ice concentration can likely be substantial in the absence
694 of regional and monthly averaging, and numerous mechanisms have been described that can
695 generate increased ice transport. Recent examples include divergent ice drift events connected to
696 anomalous circulation patterns (Zhao et al., 2018) as well as the collapse of the Beaufort High
697 (Petty, 2018; Moore et al., 2018), both of which may become more common in the future due to
698 preconditioning of the icepack and further intrusion of mid-latitude cyclones into the Arctic.
699

700 This study offers a unique contribution by focusing on the projected transient evolution
701 of Arctic sea ice variability throughout the year, as characterized by its response to external
702 greenhouse forcing superimposed on short-term internal variability. A recent study (Olonscheck
703 and Notz, 2017) also identified an overall increase in projected variability of summertime sea ice
704 area in CMIP5, but this conclusion was not consistent across all models, possibly because the
705 analysis did not incorporate the pronounced changes in variability over time as the ice pack di-
706 minishes. Increased inter-annual variability in the CESM Large Ensemble as sea ice declines
707 most rapidly is an important result that needs to be accounted for as the ice-free season expands
708 and the timing of maximum variability shifts from September. We also confirm that this relation-
709 ship is maintained across CMIP5 models, suggesting that the responsible mechanisms reported
710 here may apply more generally. These results have important implications for marine navigation
711 going forward, indicating that the otherwise auspicious transition to diminished sea ice in every

Deleted: 6

Deleted: y

Deleted: both exceed in

Deleted: at

Deleted: 6

Deleted: 6

Deleted: predicted

Deleted: are robust

Deleted: suggesting

721 month may be accompanied by a confounding increase in inter-annual variability of the ice cover
722 before the ice disappears completely.

Deleted: will

723
724
725

726 **Acknowledgements**

727

728 Support was provided by the NOAA Climate Program Office under Climate Variability and Pre-
729 dictability Program grant NA15OAR4310166. This project is partially funded by the Joint Insti-
730 tute for the Study of the Atmosphere and Ocean (JISAO) under NOAA Cooperative Agreement
731 NA10OAR4320148, contribution number 2017-087, the Pacific Marine Environmental Labora-
732 tory contribution number 4671. We would like to acknowledge high-performance computing
733 support from Yellowstone (ark:/85065/d7wd3xhc) provided by NCAR's Computational and In-
734 formation Systems Laboratory, sponsored by the National Science Foundation.

735

736

738 **References**

739
740 Aksenov, Y., E. E. Popova, A. Yool, A. J. G. Nurser, T. D. Williams, L. Bertino, and J. Bergh:
741 On the future navigability of Arctic sea routes: High-resolution projections of the Arctic
742 Ocean and sea ice, *Mar. Policy*, 1–18, doi:10.1016/j.marpol.2015.12.027, 2015.
743 Bathiany, S., B. van der Bolt, M. S. Williamson, T. M. Lenton, M. Scheffer, E. H. van Nes, and
744 D. Notz: Statistical indicators of Arctic sea-ice stability – prospects and limitations,
745 *Cryosph.*, 10(4), 1631–1645, doi:10.5194/tc-10-1631-2016, 2016.
746 Bitz, C. M., and G. H. Roe: A mechanism for the high rate of sea ice thinning in the Arctic
747 Ocean, *J. Clim.*, 17(18), 3623–3632, doi:10.1175/1520-0442(2004)017, 2004.
748 Cavalieri, D. J., and C. L. Parkinson: Arctic sea ice variability and trends, 1979–2010, *Cryosph.*,
749 6(4), 881–889, doi:10.5194/tc-6-881-2012, 2012.
750 Collins, M. et al.: Long-term Climate Change: Projections, Commitments and Irreversibility.
751 Intergovernmental Panel on Climate Change, 108, 2013.
752 Comiso, J. C., W. N. Meier, and R. Gersten: Variability and trends in the Arctic Sea ice cover:
753 Results from different techniques, *J. Geophys. Res. Ocean.*, 122, 1–22,
754 doi:10.1002/2017JC012768, 2017.
755 Ding, Q., et al., Influence of high-latitude atmospheric circulation changes on summertime
756 Arctic sea ice, *Nat. Clim. Chang.*, 7, 289–295, doi:10.1038/nclimate3241, 2017.
757 Döscher, R., and T. Koenigk: Arctic rapid sea ice loss events in regional coupled climate
758 scenario experiments, *Ocean Sci. Discuss.*, 9(4), 2327–2373, doi:10.5194/osd-9-2327-
759 2012, 2012.
760 Goosse, H., O. Arzel., C.M. Bitz, A. de Montety, and M. Vancoppenolle: Increased variability of
761 the Arctic summer ice extent in a warmer climate, *Geophys. Res. Lett.*, 36, L23702,
762 doi :10.1029/2009GL040546, 2009.
763 Holland, M. M., C. M. Bitz, and B. Tremblay: Future abrupt reductions in the summer Arctic sea
764 ice, *Geophys. Res. Lett.*, 33(23), 1–5, doi:10.1029/2006GL028024, 2006.
765 Holland, M. M., C. M. Bitz, L. B. Tremblay, and D. A. Bailey: The role of natural versus forced
766 change in future rapid summer Arctic ice loss. Arctic sea ice decline: Observations,
767 projections, mechanisms, and implications, E.T. DeWeaver, C.M. Bitz, and L.B.
768 Tremblay, Eds., *Geophysical Monograph Series*, American Geophysical Union,
769 Washington, 133-150 doi:10.1029/180GM10, 2008.
770 Holland, M. M., and J. Stroeve: Changing seasonal sea ice predictor relationships in a changing
771 Arctic climate, *Geophys. Res. Lett.*, 38, L18501, doi:10.1029/2011GL049303, 2011.
772 Jahn, A., J. E. Kay, M. M. Holland, and D. M. Hall: How predictable is the timing of a summer
773 ice-free Arctic?, *Geophys. Res. Lett.*, 1–8, doi:10.1002/2016GL070067, 2016.
774 Eguíluz, V. M., J. Fernández-Gracia, X. Irigoien, and C. M. Duarte: A quantitative assessment of
775 Arctic shipping in 2010–2014, *Sci. Rep.*, 6(August), 30682, doi:10.1038/srep30682,
776 2016.
777 Eisenman, I.: Geographic muting of changes in the Arctic sea ice cover, *Geophys. Res. Lett.*,
778 37(16), doi:10.1029/2010GL043741, 2010.
779 [Hunke, E. C., and W. H. Lipscomb: CICE: The Los Alamos sea ice model, documentation and
780 software user’s manual, version 4.1. Los Alamos National Laboratory Tech. Rep. LACC-
781 06-012, 76 pp., 2010.](#)
782 [Kay, J. E. et al.: The Community Earth System Model \(CESM\) Large Ensemble Project: A
783 Community Resource for Studying Climate Change in the Presence of Internal Climate](#)

Deleted: ¶

Deleted: ¶

788 Variability, *Bull. Am. Meteorol. Soc.*, 96(8), 1333–1349, doi:10.1175/BAMS-D-13-
789 00255.1, 2015.

790 Kay, J. E., M. M. Holland, and A. Jahn: Inter-annual to multi-decadal Arctic sea ice extent trends
791 in a warming world. *Geophys. Res. Lett.*, 38, L15708, doi:10.1029/2011GL048008,
792 2011.

793 Kelleher, M., and J. Screen: Atmospheric precursors of and response to anomalous Arctic sea ice
794 in CMIP5 models, *Adv. Atmos. Sci.*, 35(27), doi.org/10.1007/s00376-017-7039-9.

795 Khon, V. C., I. I. Mokhov, M. Latif, V. A. Semenov, and W. Park: Perspectives of Northern Sea
796 Route and Northwest Passage in the twenty-first century, *Clim. Change*, 100(3), 757–
797 768, doi:10.1007/s10584-009-9683-2, 2010.

798 Kwok, R., and D. A. Rothrock: Decline in Arctic sea ice thickness from submarine and ICESat
799 records: 1958-2008, *Geophys. Res. Lett.*, 36(15), doi:10.1029/2009GL039035.

800 Kwok, R., G. F. Cunningham, M. Wensnahan, I. Rigor, H. J. Zwally, and D. Yi: Thinning and
801 volume loss of the Arctic Ocean sea ice cover: 2003-2008, *J. Geophys. Res. Ocean.*,
802 114(7), 2003–2008, doi:10.1029/2009JC005312, 2009.

803 [Kwok, R. L. T., Pederse, P., Gudmandsen, and S. S. Pang: Large sea ice outflow into the Nares](#)
804 [strait in 2007, *geophys. Res. Lett.* 37, L03502, DOI:10.1029/2009GL041872, 2010.](#)

805 Labe, Z., Magnusdottir, G., and H. Stern: Variability of Arctic Sea Ice Thickness Using
806 PIOMAS and the CESM Large Ensemble, *J. Climate*, 31, 3233–3247,
807 [DOI.ORG/10.1175/JCLI-D-17-0436.1](#), 2018.

808 Lang, A., S. Yang, and E. Kaas: Sea ice thickness and recent Arctic warming, *Geophys. Res.*
809 *Lett.*, 44, doi:10.1002/2016GL071274, 2017.

810 Li, D., R. Zhang, and T. Knutson: Comparison of Mechanisms for Low-Frequency Variability of
811 Summer Arctic Sea Ice in Three Coupled Models, *J. Climate*, 31, 1205–
812 1226, [DOI.ORG/10.1175/JCLI-D-16-0617.1](#), 2018.

813 Maslanik, J. A., M. C. Serreze, and R. G. Barry: Recent decreases in Arctic summer ice cover
814 and linkages to atmospheric circulation anomalies, *Geophys. Res. Lett.*, 23(13), 1677–
815 1680, doi:10.1029/96GL01426, 1996.

816 Maslanik, J., S. Drobot, C. Fowler, W. Emery, and R. Barry: On the Arctic climate paradox and
817 the continuing role of atmospheric circulation in affecting sea ice conditions, *Geophys.*
818 *Res. Lett.*, 34(3), 2–5, doi:10.1029/2006GL028269, 2007a.

819 Maslanik, J. A., C. Fowler, J. Stroeve, S. Drobot, J. Zwally, D. Yi, and W. Emery: A younger,
820 thinner Arctic ice cover: Increased potential for rapid, extensive sea-ice loss, *Geophys.*
821 *Res. Lett.*, 34(24), 2004–2008, doi:10.1029/2007GL032043, 2007b.

822 Maslanik, J., J. Stroeve, C. Fowler, and W. Emery: Distribution and trends in Arctic sea ice age
823 through spring 2011, *Geophys. Res. Lett.*, 38(13), 2–7, doi:10.1029/2011GL047735,
824 2011.

825 Massonnet, F., T. Fichefet, H. Goosse, C. M. Bitz, G. Philippon-Berthier, M. M. Holland, and P.
826 Y. Barriat: Constraining projections of summer Arctic sea ice, *Cryosphere*, 6(6), 1383–
827 1394, doi:10.5194/tc-6-1383-2012, 2012.

828 [Massonnet, F., M. Vancoppenolle, H. Goosse, D. Docquier, T. Fifechet, and E. Blanchard-](#)
829 [Wrigglesworth: Arctic sea-ice change tied to its mean state through thermodynamic](#)
830 [processes. *Nat. Clim. Change*, 8, 599-603, 2018.](#)

831 Maykut, G. A.: Energy exchange over young sea ice in the central Arctic, *J. Geophys. Res.*,
832 83(C7), 3646, doi:10.1029/JC083iC07p03646, 1978.

833 Melia, N., K. Haines, and E. Hawkins: Sea ice decline and 21st century trans-Arctic shipping
834 routes, *Geophys. Res. Lett.*, 43(18), 9720–9728, doi:10.1002/2016GL069315, 2016.

835 Moore, G. W. K., Schweiger, A., Zhang, J., and M. Steele: Collapse of the 2017 winter Beaufort
836 High: A response to thinning sea ice? *Geophysical Research Letters*, 45, 2860–2869,
837 doi.org/10.1002/2017GL076446, 2018

838 Nghiem, S. V., I. G. Rigor, D. K. Perovich, P. Clemente-Colón, J. W. Weatherly, and G. Neu-
839 mann: Rapid reduction of Arctic perennial sea ice, *Geophys. Res. Lett.*, 34(19), 1–6,
840 doi:10.1029/2007GL031138, 2007.

841 Notz, D.: The future of ice sheets and sea ice: between reversible retreat and unstoppable loss.,
842 *Proc. Natl. Acad. Sci. U. S. A.*, 106(49), 20590–5, doi:10.1073/pnas.0902356106, 2009.

843 Notz, D., and J. Marotzke: Observations reveal external driver for Arctic sea-ice retreat,
844 *Geophys. Res. Lett.*, 39(8), 1–6, doi:10.1029/2012GL051094, 2012.

845 Notz, D., and J. Stroeve: Observed Arctic sea-ice loss directly follows anthropogenic CO₂
846 emission, *Science*, 354(6313), 747–750, doi:10.1126/science.aag2345, 2016.

847 Olonscheck, D., and D. Notz: Consistently estimating internal variability from climate model
848 simulations. *J. Clim.*, 30, 9555–9573, 2017.

849 Overland, J. E., and M. Wang: When will the summer Arctic be nearly sea ice free?, *Geophys.*
850 *Res. Lett.*, 40(10), 2097–2101, doi:10.1002/grl.50316, 2013.

851 Perovich, D. K., B. Light, H. Eicken, K. F. Jones, K. Runciman, and S. V. Nghiem: Increasing
852 solar heating of the Arctic Ocean and adjacent seas, 1979–2005: Attribution and role in
853 the ice-albedo feedback, *Geophys. Res. Lett.*, 34(19), 1–5, doi:10.1029/2007GL031480,
854 2007.

855 Petty, A. A.: A possible link between winter Arctic sea ice decline and a collapse of the Beaufort
856 High? *Geophysical Research Letters*, 45, 2879–2882,
857 [DOI.ORG/10.1002/2018GL077704](https://doi.org/10.1002/2018GL077704), 2018.

858 Ridley, J. K., R. A. Wood, A. B. Keen, E. Blockley, and J. A. Lowe: Brief Communication:
859 Does it matter exactly when the Arctic will become ice-free?, *Cryosph. Discuss.*,
860 (March), 1–4, doi:10.5194/tc-2016-28, 2016.

861 Sanderson, B. M., Xu, Y., Tebaldi, C., Wehner, M., O'Neill, B., Jahn, A., Pendergrass, A. G.,
862 Lehner, F., Strand, W. G., Lin, L., Knutti, R., and Lamarque, J. F.: Community climate
863 simulations to assess avoided impacts in 1.5 and 2 °C futures, *Earth Syst. Dynam.*, 8,
864 827–847, <https://doi.org/10.5194/esd-8-827-2017>, 2017.

865 Sanderson, B. M., K. W. Oleson, W. G. Strand, F. Lehner, and B. C. O'Neill: A new ensemble of
866 GCM simulations to assess avoided impacts in a climate mitigation scenario, *Clim.*
867 Change, 146(3–4), 303–318, 2018.

868 Serreze, M. C., and J. C. Stroeve: Arctic sea ice trends, variability and implications for seasonal
869 ice forecasting, *Philos. Trans. R. Soc. A Math. Phys. Eng. Sci.*, 373(2045), 20140159,
870 doi:10.1098/rsta.2014.0159, 2015.

871 Stephenson, S. R., L. C. Smith, L. W. Brigham, and J. A. Agnew: Projected 21st-century
872 changes to Arctic marine access, *Clim. Change*, 118(3–4), 885–899, doi:10.1007/s10584-
873 012-0685-0, 2013.

874 Stammerjohn, S., R. Massom, D. Rind, and D. Martinson: Regions of rapid sea ice change: An
875 inter-hemispheric seasonal comparison, *Geophys. Res. Lett.*, 39(6), L06501,
876 doi:10.1029/2012GL050874, 2012.

877 Stroeve, J. C., M. C. Serreze, M. M. Holland, J. E. Kay, J. Malanik, and A. P. Barrett: The
878 Arctic's rapidly shrinking sea ice cover: a research synthesis, *Clim. Change*, 110(3–4),
879 1005–1027, doi:10.1007/s10584-011-0101-1, 2012.

880 Stroeve, J., M. M. Holland, W. Meier, T. Scambos, and M. Serreze: Arctic sea ice decline: Faster
881 than forecast, *Geophys. Res. Lett.*, 34(9), 1–5, doi:10.1029/2007GL029703, 2007.

882 Swart, N. C., J. C. Fyfe, E. Hawkins, J. E. Kay, and A. Jahn: Influence of internal variability on
883 Arctic sea-ice trends, *Nat. Clim. Chang.*, 5(2), 86–89, doi:10.1038/nclimate2483, 2015.

884 Tietsche, S., D. Notz, J. H. Jungclaus, and J. Marotzke: Recovery mechanisms of Arctic summer
885 sea ice, *Geophys. Res. Lett.*, 38(2), 1–4, doi:10.1029/2010GL045698, 2011.

886 Wang, M., and J. E. Overland: A sea ice free summer Arctic within 30 years? *Geophys. Res.*
887 *Lett.*, 36, L07502, doi:10.1029/2009GL037820, 2009.

888 Wang, M., and J. E. Overland: A sea ice free summer Arctic within 30 years: An update from
889 CMIP5 models, *Geophys. Res. Lett.*, 39(18), doi:10.1029/2012GL052868, 2012.

890 Wang, M., and J. E. Overland: Projected future duration of the sea-ice-free season in the Alaskan
891 Arctic, *Prog. Oceanogr.*, 136, 50–59, doi:10.1016/j.pocean.2015.01.001, 2015.

892 Wernli, H., and L. Papritz: Role of polar anticyclones and mid-latitude cyclones for Arctic
893 summertime sea-ice melting, *Nat. Geos.*, 11, 108–113, doi:10.1038/s41561-017-0041-0,
894 2018.

895 Woodgate, R. A., T. J. Weingartner, and R. Lindsay: Observed increases in Bering Strait oceanic
896 fluxes from the Pacific to the Arctic from 2001 to 2011 and their impacts on the Arctic
897 Ocean water column, *Geophys. Res. Lett.*, 39, L24603, doi:10.1029/2012GL054092,
898 2012.

899 Zhao, J., D. Barber, S. Zhang, Q. Yang, X. Wang, and H. Xie: Record Low Sea-Ice
900 Concentration in the Central Arctic during Summer 2010, *Adv. Atmos. Sci.*, 35(January),
901 106–115, doi:10.1007/s00376-017-7066-6, 2018.

902
903
904

Deleted: Zhao, J., D. Barber, S. Zhang, Q. Yang, X. Wang, and H. Xie (2018), Record Low Sea-Ice Concentration in the Central Arctic during Summer 2010, *Adv. Atmos. Sci.*, 35(January), 106–115, doi:10.1007/s00376-017-7066-6.

910
911
912
913
914
915
916
917
918
919
920
921
922
923
924
925
926
927
928
929
930
931
932
933
934
935
936
937
938
939
940
941
942
943
944
945
946
947

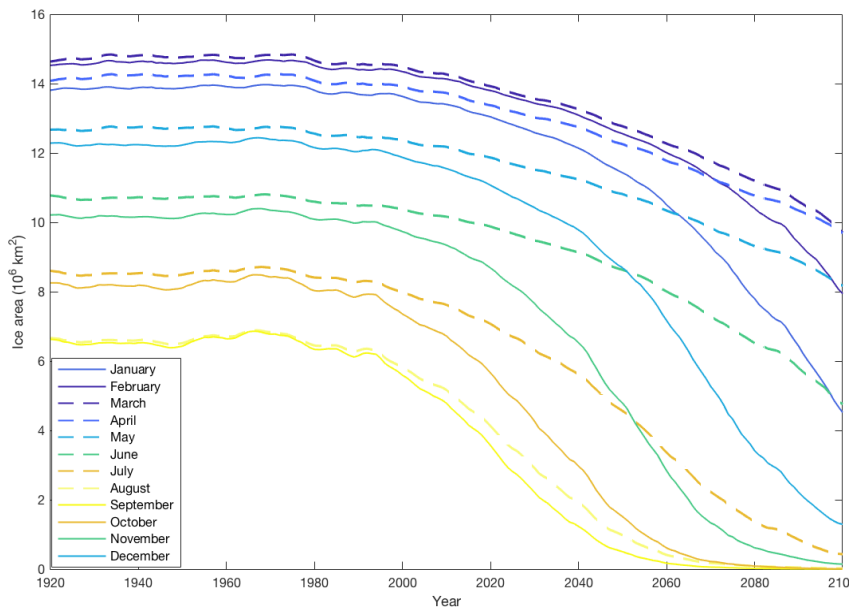


Figure 1: The CESM-LE ensemble mean time series of monthly sea ice area ($\text{km}^2 \times 10^6$).

Deleted:

Figure S1: The CESM-LE ensemble mean time series of monthly sea ice area ($\text{km}^2 \times 10^6$).

<object>

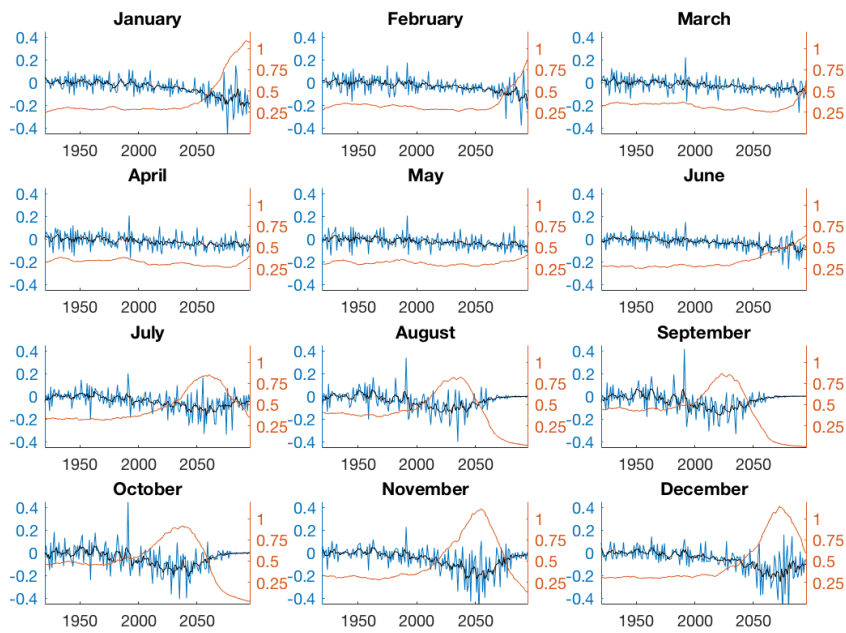
Figure S12: Map of the total number of ensemble members where the standard deviation of the 10-year time series of ice area within each grid cell exceeds 30% within a) September and b) December's decade of maximum variability.

Formatted: None, Font: (Default) Times New Roman, Italic, Underline color: Dark Gray, Font color: Dark Gray, Check spelling and grammar

Formatted: Font: (Default) Times New Roman, 12 pt

Moved (insertion) [1]

976
977
978
979
980
981
982
983
984
985
986
987
988
989
990
991
992
993
994
995
996
997
998
999
1000
1001
1002
1003
1004
1005
1006
1007
1008
1009
1010
1011
1012
1013
1014
1015
1016
1017



Formatted: Font: (Default) Times New Roman, 12 pt

Figure 2: The CESM-LE ensemble mean of the 1-year differences in sea ice area (blue; million km²) with their 5-year running mean overlaid (black) and the running standard deviation of the interannual change in sea ice area (gold; million km²).

1018
1019
1020
1021
1022
1023
1024
1025
1026
1027
1028
1029
1030
1031
1032
1033
1034
1035
1036
1037
1038
1039
1040
1041
1042
1043
1044
1045
1046
1047
1048
1049
1050
1051
1052
1053
1054
1055

Formatted: Font: (Default) Times New Roman, 12 pt

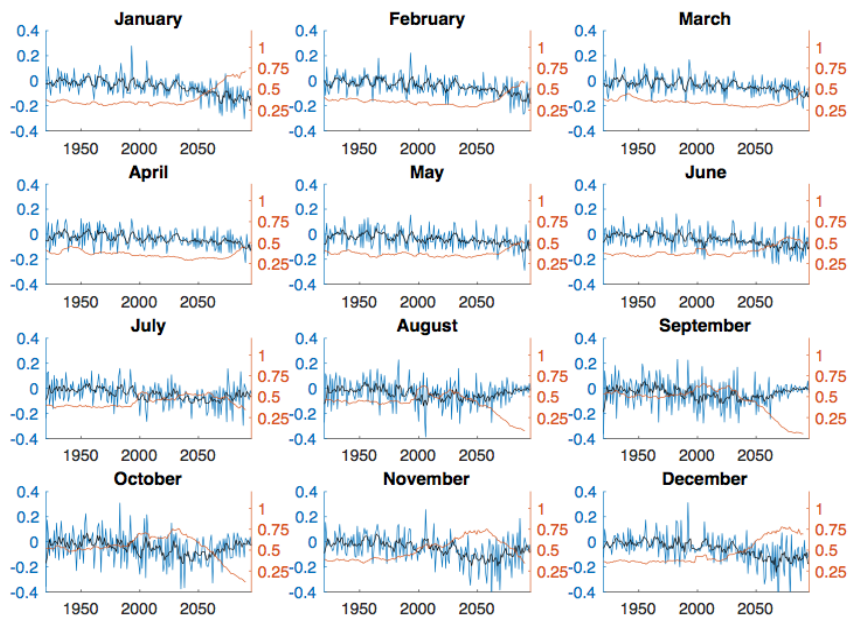
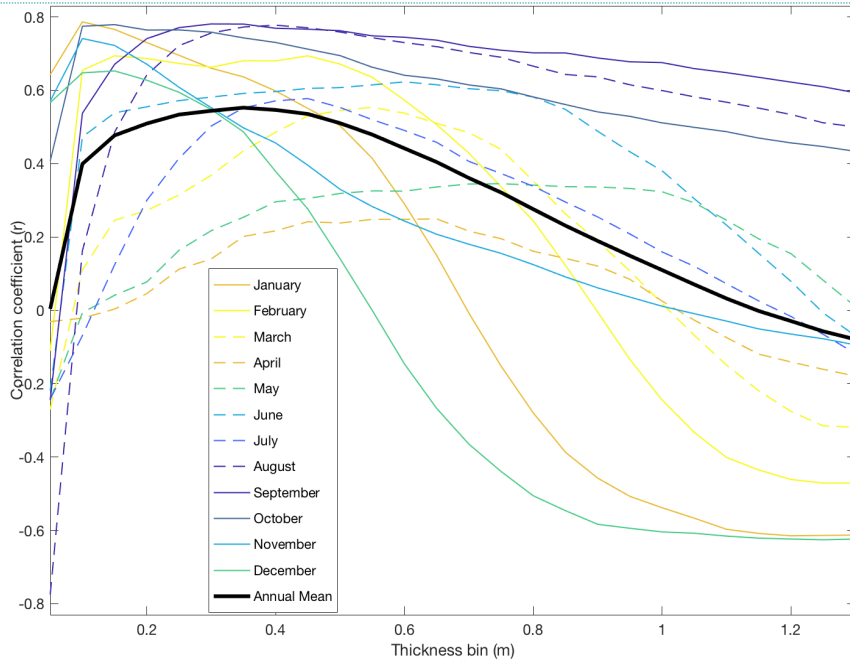


Figure 3: As in Fig. 2, but for the ensemble mean from 12 CMIP5 models' sea ice area.

1056
1057
1058
1059
1060
1061
1062
1063
1064
1065
1066
1067
1068
1069
1070
1071
1072
1073
1074
1075
1076
1077
1078
1079
1080
1081
1082
1083
1084
1085
1086
1087
1088
1089



Formatted: Font: (Default) Times New Roman, 14 pt, Bold

Figure 4: Monthly correlation coefficient (r) of the 2000-2100 10-year running standard deviation of 1-year difference in sea ice area with mean grid cell ice thickness binned every 0.05 m of thickness.

1090
1091
1092
1093
1094
1095
1096
1097
1098
1099
1100
1101
1102
1103
1104
1105
1106
1107
1108
1109
1110
1111
1112
1113
1114
1115
1116
1117
1118
1119
1120
1121
1122
1123
1124
1125
1126
1127
1128
1129
1130
1131
1132
1133
1134

Formatted: Font: Underline color: Red, Font color: Red

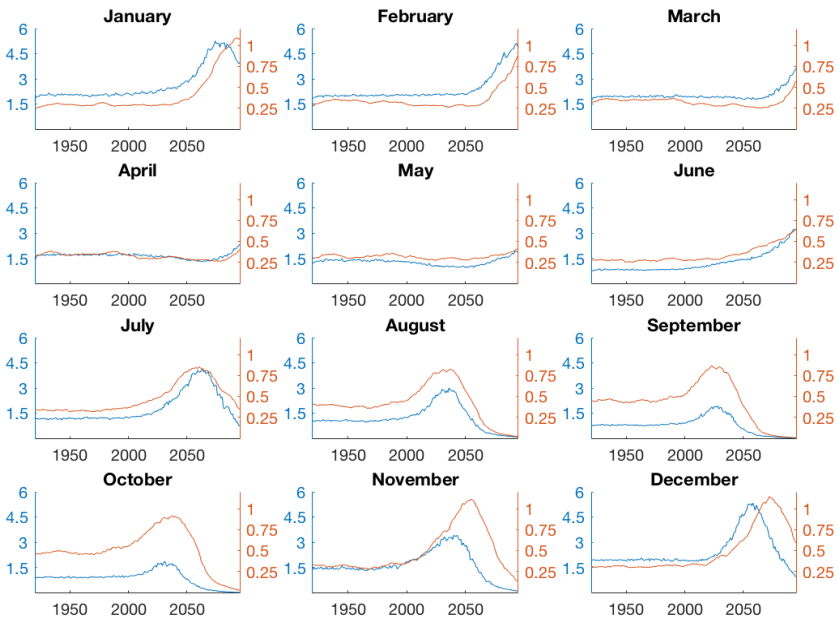
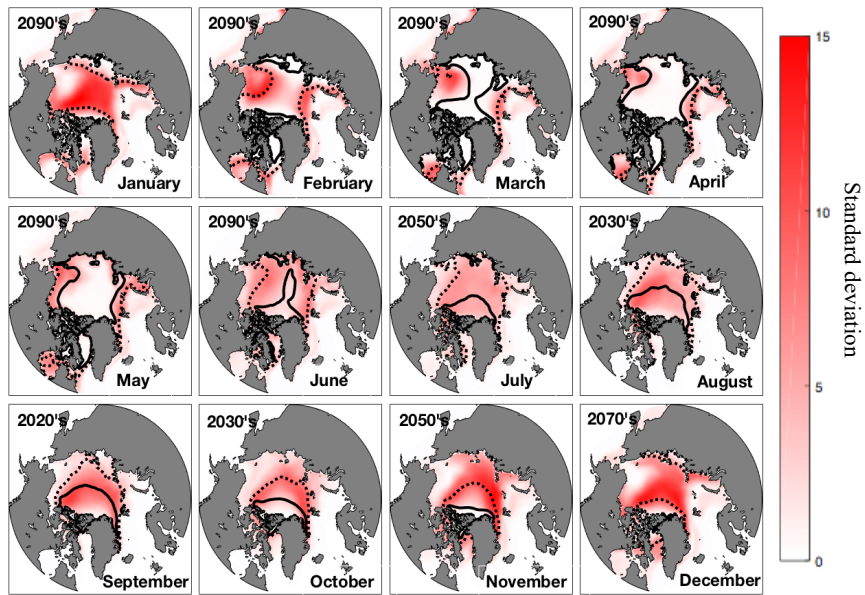


Figure 5: The CESM-LE ensemble mean of the 10-year running standard deviation of 1-year difference in sea ice area from Figure 1 (gold; million km²) and the ensemble mean total area of grid cells with mean ice thickness between 0.2 m and 0.6 m (blue; million km²).

1|135
1|136
1|137
1|138
1|139
1|140

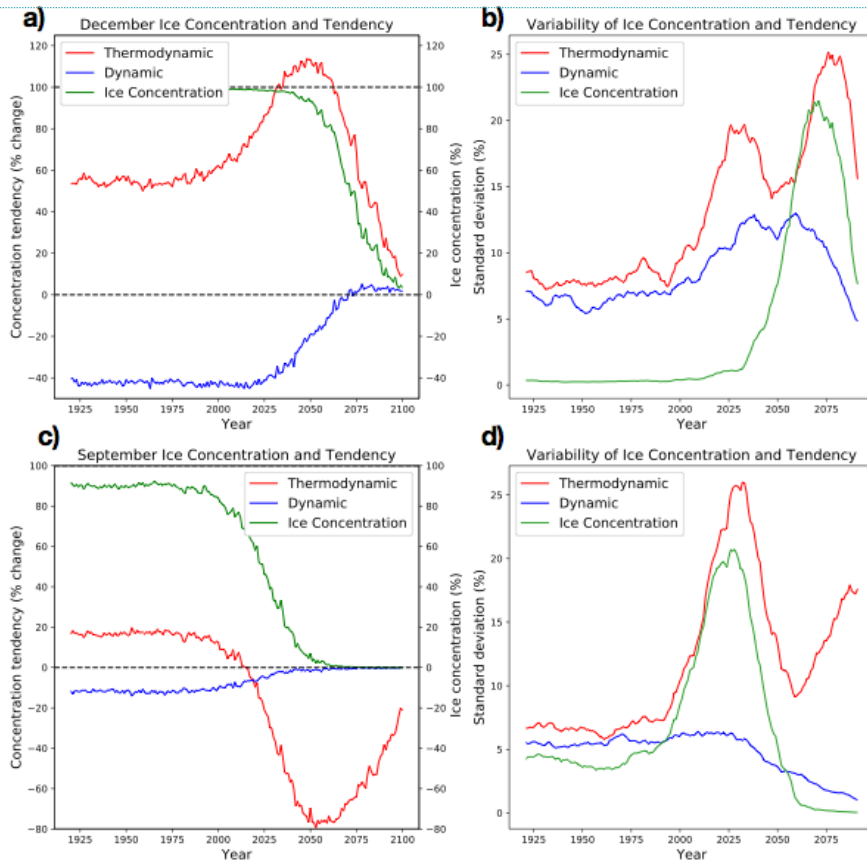
Formatted: Font: (Default) Times New Roman, 12 pt



1|141
1|142
1|143
1|144
1|145
1|146
1|147
1|148
1|149
1|150
1|151
1|152
1|153
1|154
1|155
1|156
1|157

Figure 6: Monthly ensemble average in CESM-LE of the 10-year running standard deviation of ice concentration (%) in the decade when ice area variability is maximum. Mean 0.2 m and 0.6 m ice thicknesses are indicated by the dotted and solid contours, respectively.

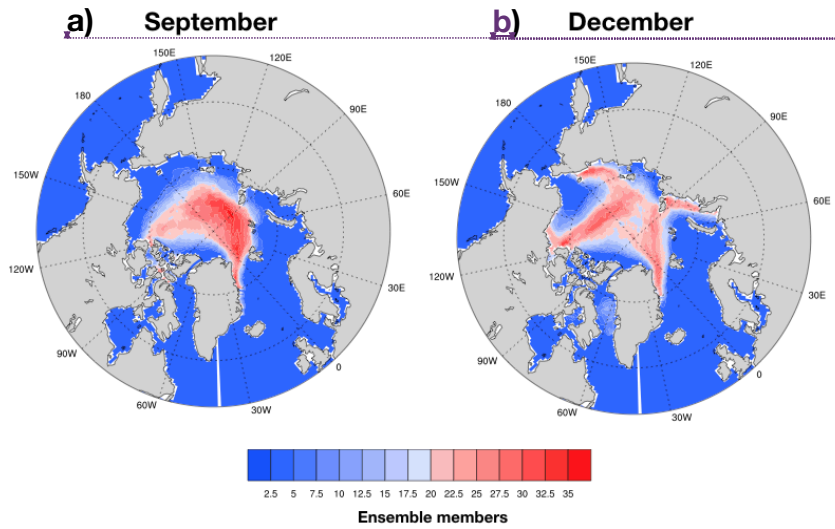
1158
 1159
 1160
 1161
 1162
 1163
 1164
 1165
 1166
 1167
 1168
 1169
 1170
 1171
 1172
 1173
 1174
 1175
 1176
 1177
 1178
 1179
 1180
 1181
 1182
 1183
 1184
 1185
 1186
 1187
 1188
 1189
 1190
 1191
 1192
 1193
 1194
 1195
 1196
 1197
 1198
 1199
 1200
 1201
 1202
 1203
 1204



Formatted: Font: (Default) Times New Roman, 12 pt

Figure 7: Time series of ensemble-mean a) September ice concentration (%) and July-September averaged concentration tendency (% day⁻¹) from dynamics and thermodynamics, and b) the 10-year running standard deviation of: the inter-annual difference in ice concentration (%) and July-September ice concentration tendency from dynamics and thermodynamics (% day⁻¹). The same information is presented in c) and d) for December concentration and October-December ice concentration tendency terms.

1205
1206
1207
1208
1209
1210
1211
1212
1213
1214
1215
1216
1217
1218
1219
1220
1221
1222
1223
1224
1225
1226
1227
1228
1229
1230
1231
1232
1233
1234
1235
1236
1237



- Deleted: (
- Formatted: Font: 16 pt
- Deleted: (
- Formatted: Font: 16 pt, Font color: Auto
- Formatted: Font color: Auto
- Deleted: a
- Formatted: Font: 16 pt

Figure S1: Map of the total number of ensemble members where the standard deviation of the 10-year time series of ice area within each grid cell exceeds 30% within a) September's and b) December's decade of maximum variability.

Page 5: [1] Deleted	Steve Vavrus	9/3/18 9:52:00 AM
Page 5: [2] Deleted	Steve Vavrus	9/3/18 10:15:00 AM
Page 6: [3] Deleted	≥÷÷	9/2/18 2:53:00 PM
Page 6: [3] Deleted	≥÷÷	9/2/18 2:53:00 PM
Page 6: [3] Deleted	≥÷÷	9/2/18 2:53:00 PM
Page 6: [4] Deleted	≥÷÷	9/2/18 2:54:00 PM
Page 6: [4] Deleted	≥÷÷	9/2/18 2:54:00 PM
Page 6: [4] Deleted	≥÷÷	9/2/18 2:54:00 PM
Page 6: [5] Deleted	Stephen Vavrus [2]	8/25/18 9:18:00 AM
Page 6: [5] Deleted	Stephen Vavrus [2]	8/25/18 9:18:00 AM
Page 6: [6] Deleted	Stephen Vavrus [2]	8/25/18 9:20:00 AM
Page 6: [6] Deleted	Stephen Vavrus [2]	8/25/18 9:20:00 AM
Page 6: [7] Deleted	Muyin Wang	8/24/18 12:00:00 AM
Page 6: [8] Deleted	Steve Vavrus	9/3/18 9:57:00 AM
Page 6: [9] Deleted	≥÷÷	9/2/18 2:53:00 PM
Page 6: [9] Deleted	≥÷÷	9/2/18 2:53:00 PM
Page 6: [10] Deleted	Steve Vavrus	9/3/18 10:01:00 AM
Page 6: [11] Deleted	≥÷÷	9/2/18 2:50:00 PM
Page 6: [11] Deleted	≥÷÷	9/2/18 2:50:00 PM